Selenoprotein K contributes to CD36 subcellular trafficking in hepatocytes by accelerating nascent COPII vesicle formation and aggravates hepatic steatosis

Mengyue You [a], Fan Wu [a], Meilin Gao [a], Mengyue Chen [a], Shu Zeng [a], Yang Zhang [a], Wei Zhao [a], Danyang Li [a], Li Wei [a], Xiong Z. Ruan [a,b,**], Yaxi Chen [a,*]

[a] *Centre for Lipid Research & Key Laboratory of Molecular Biology for Infectious Diseases (Ministry of Education), Institute for Viral Hepatitis, Department of Infectious Diseases, The Second Affiliated Hospital, Chongqing Medical University, 400016, Chongqing, China*
[b] *John Moorhead Research Laboratory, Centre for Nephrology, University College London Medical School, Royal Free Campus, University College London, London, NW3 2PF, United Kingdom*

ABSTRACT

SelenoproteinK (SelK), an endoplasmic reticulum (ER) - resident protein, possesses the property of mediate oxidation resistance and ER - associated protein degradation (ERAD) in several tissues. Here, we found that increased SelK markedly promotes fatty acid translocase (CD36) subcellular trafficking and aggravates lipid accumulation in hepatocytes. We demonstrated that SelK is required for the assembly of COPII vesicles and accelerates transport of palmitoylated-CD36 from the ER to Golgi, thus facilitating CD36 plasma membrane distribution both in vivo and *in vitro*. The mechanism is that SelK increases the stability of Sar1B and triggers CD36-containing nascent COPII vesicle formation, consequently, promotes CD36 subcellular trafficking. Furthermore, we verified that the intervention of SelK SH3 binding domain can inhibit the vesicle formation and CD36 subcellular trafficking, significantly ameliorates NAFLD in mice. Collectively, our findings disclose an unexpected role of SelK in regulating NAFLD development, suggesting that targeting the SelK of hepatocytes may be a new therapeutic strategy for the treatment of NAFLD.

1. Introduction

Non-alcoholic fatty liver disease (NAFLD) is associated with metabolic disorders and affects approximately 25% of the global population [1,2]. NAFLD involves a broad spectrum of pathological conditions ranging from simple steatosis (SS) and non-alcoholic steatohepatitis (NASH) to fibrosis and ultimately cirrhosis and hepatocellular carcinoma (HCC) [3,4]. The pathogenesis of NAFLD is always a fascinating and challenging topic that requires further studies, since there are limited therapeutic options available to patients.

CD36 is a widely expressed transmembrane glycoprotein which serves many functions in lipid metabolism and signaling [5–8]. Anomalously elevated CD36 increases fatty acid (FA) uptake and lipid accumulation in liver cells, drives hepatosteatosis onset and oxidative stress, indisputably contributes to the progression of NAFLD in rodents and

patients [9]. Our previous studies have demonstrated that the localization of fatty acid translocase (FAT/CD36) on the hepatocellular plasma membrane plays a crucial role in NAFLD pathogenesis [10,11]. Post-translational modification, such as palmitoylation, has been considered to regulate the membrane association and stable expression of transmembrane proteins [12,13]. CD36 is palmitoylated at both N-terminal (Cys3 and Cys7) and C-terminal (Cys464 and Cys466) residues. Inhibition of CD36 palmitoylation via mutating its four palmitoylation sites significantly reduced membrane localization of CD36 and ameliorated NAFLD [10,14]. However, the molecular and biochemical mechanisms underlying the regulation of CD36 subcellular trafficking are far from clear.

Selenoprotein is a small but vital family of proteins, with selenium as an essential trace element in the selenocysteine (Sec) amino acid residue [15,16]. The human selenoproteome consists of at least 25

selenoproteins [17]. The hepatic transcriptome and quantitative histomorphometry demonstrated that individual selenoprotein genes were highly expressed in steatosis patients [18]. Among these, we focused on selenoprotein K (SelK), a single-pass transmembrane protein that resides in the endoplasmic reticulum (ER) membrane [19], which has been reported to an emerging role of playing a part in protein palmitoylation [20]. Human SelK is a 94-amino-acid protein with Sec residing at the penultimate position [16]. It has been shown that SelK is expressed predominantly in the heart and skeletal muscle, but other tissues, such as the liver, pancreas, and placenta, also have detectable levels of SelK [21]. Previous findings provide mechanistic insight into that *SelK* knockout mice exhibit compromised immunity and the overexpression of SelK decreased the levels of intracellular ROS and protected cardiomyocytes and neurons against exogenously imposed oxidative stress [21–23]. Although SelK may perform an oxidation resistance function in several tissues, whether SelK takes part in the regulation of hepatic steatosis is entirely unknown. Notably, recent studies reported that SelK act as a cofactor of DHHC6 (Asp-His-His-Cys) palmitoyltransferase in regulating palmitoylation of 1,4,5-triphosphate receptor (IP3R) and CD36, in immune cells and macrophages respectively [24,25]. Considering the importance of palmitoylation in regulating protein trafficking and subcellular localization, it is worth further exploring whether SelK participates in CD36 subcellular localization in hepatocytes and, more in-depth, it regulates CD36 subcellular trafficking mechanism.

In the current study, we found that SelK expression is upregulated in the livers of mice with NAFLD and increased SelK markedly promotes CD36 subcellular trafficking and aggravates lipid accumulation in hepatocytes. To elaborate the mechanism of CD36 subcellular localization in hepatocytes, we investigated the role of SelK in the trafficking of CD36 cargo between subcellular compartments. We demonstrated that SelK facilitates the recruitment and assembly of COPII vesicles, which control the vesicular transport process from the ER to the Golgi apparatus, by regulating the degradation of Sar1B. SelK accelerates the ER-Golgi trafficking of CD36 by concentrating palmitoylated-CD36 into nascent COPII vesicles. Our findings suggest that SelK performs a novel function in CD36 subcellular trafficking in hepatocytes and may provide a potential therapeutic strategy for NAFLD.

2. Materials and methods

2.1. Animal experiments

Animal experiments were conducted in accordance with ethical guidelines of the Institutional Animal Care and Use Committee of Chongqing Medical University, and the investigation conforms to the Guidelines for the Care and Use of Laboratory Animals published by the US National Institutes of Health (NIH Publication No. 85–23, revised 1996). The CD36 knockout (CD36KO) mice with a C57BL/6J background were kindly provided by Dr Maria Febbraio (Lerner Research Institute, U.S.). All mice were housed with food and water available ad libitum in a 12-h light/dark environment. All animals were sacrificed during the light cycle, and none were involved in previous studies.

For the NAFLD models, eight-week-old male C57BL/6J mice were fed a high-fat diet (HFD) (n = 6) or normal chow diet (NCD) (n = 6) for 16 weeks (research diets 12492 and 12109B). In some experiments, 8-week-old male CD36KO mice were injected with NC adeno-associated virus AAV2/8 vectors (n = 6), wt-CD36 adeno-associated virus AAV2/8 vectors (n = 6) and AA-SS adeno-associated virus AAV2/8 vectors (n = 6) in the tail vein and maintained on a HFD for eight weeks. In rescue experiments (Fig. 8), 8-week-old male C57BL/6J mice were injected with NC adeno-associated virus AAV2/8 vectors (n = 6), SelK-full length adeno-associated virus AAV2/8 vectors (n = 6) and SelK-SH3 binding domain truncated adeno-associated virus AAV2/8 vectors (n = 6) in the tail vein and fed a HFD for eight weeks.

2.2. Cell cultures

HepG2 and Huh7 cells were cultured in Dulbecco's modified Eagle's medium (DMEM, HyClone, Logan, UT (4.5 g/L glucose) supplemented with 10% (v/v) FBS (Natocor, Corcovado, Argentina), 100 U/ml penicillin, and 100 mg/ml streptomycin at 37 °C in an atmosphere of 5% CO_2. All cell lines were mycoplasma free.

2.3. Lentivirus production and stable cell lines

For lentiviral overexpression, His-Tag SelK-full length or SelK SH3 binding domain truncated (SH3 BD TRUNC) lentivirus was transfected into HepG2 or Huh7 cells. Stable cell lines expressing SelK and SelK SH3 BD TRUNC were obtained by sorting the cells using puromycin treatment. For the stable knockdown of SelK, HepG2 or Huh7 cells were incubated with shSelK lentivirus (MOI 10) for 48 h at 37 °C and selected for the stable expression of shSelK using puromycin.

2.4. Histology, Oil red O

Paraffin-embedded tissue sections were routinely stained with hematoxylin and eosin (HE) using standard protocols. The frozen tissue sections were incubated in Oil Red O reagent for 15 min, followed by hematoxylin counterstaining for 1 min. All images were captured using a Zeiss microscope. Image analysis procedures were performed with ImageJ software.

2.5. Quantitative real-time PCR

Total RNA was isolated from cells and mouse liver tissue, and quantitative real-time PCR was performed as previously described [26], using SYBR master mix (Takara). After reverse transcription, all reactions were performed in triplicate, and the mean range of variation for all values was $0.20 \pm 0.03\%$. The relative amount of each mRNA was calculated by using the comparative threshold cycle (CT) method. β-actin mRNA was used as the invariant control.

2.6. Western blots

Protein from tissue and cell lysates was extracted with RIPA buffer. For Western blotting analysis, equal amounts of protein were loaded onto SDS-PAGE gels and electro-transferred to polyvinyl difluoride (PVDF) membranes (Millipore, Darmstadt, Germany). Membranes were blocked with 3% BSA for 1 h at room temperature and incubated with primary antibodies overnight at 4 °C. The following primary antibodies were used: anti-CD36 (1:2000; #NB400-144, Novus Biologicals), anti-β actin (1:3000, #20536-1-AP, Proteintech), anti-SelK (1:2000; #ab139949, Abcam), anti-Calnexin (1:2000; #2679S, Cell Signaling Technology), anti-GM130 (1:2000; #11308-1-AP, Proteintech), anti-TGN46 (1:2000; #MA3-063, Invitrogen), anti-Caveolin-1 (1:2000; #16447-1-AP, Proteintech), anti-SAR1A (1:1000; #15350-1-AP, Proteintech), anti-SAR1B (1:1000; #22292-1-AP, Proteintech), anti-TFG (1:1000; #11571-1-AP, Proteintech), anti-SEC24 (1:1000; #15958-1-AP, Proteintech), anti-SEC13 (1:1000; #15397-1-AP, Proteintech), anti-SEC31A (1:1000; #17913-1-AP, Proteintech), anti-SEC12 (1:1000; #10146-2-AP, Proteintech), anti-SEC23 (1:1000; # A12101, ABclonal), anti-GAPDH (1:5000; #60004-1-Ig, Proteintech). After being washed three times (10 min each time) with TBST, the blots were incubated with appropriate HRP-conjugated secondary antibodies at room temperature for 1 h and subsequently washed with TBST three times (15 min each). Images of the Western blots were detected by using an ECL reagent (Clarity Western ECL, Bio-Rad Laboratories) and quantified by Fiji ImageJ software.

2.7. Immunofluorescence

After the indicated treatments as described in the figure legends, frozen slices or cells were fixed with 4% paraformaldehyde for 15 min at 37 °C and incubated with 0.2% Triton X100 for 15 min at room temperature. After blocking with 3% bovine serum albumin, the slices were incubated with primary antibodies. The following primary antibodies were used: anti-CD36 (#NB600-1423, Novus Biologicals), anti-SELK (#ab121276, Abcam), anti-SEC24 (#15958-1-AP, Proteintech), anti-His-Tag (#12698S, Cell Signaling Technology), anti-Calnexin (#66903-1-Ig, Proteintech), anti-GM130 (#11308-1-AP, Proteintech), anti-Golgin97 (#12640-1-AP, Proteintech), anti-TGN46 (#MA3-063, Invitrogen). After overnight incubation at 4 °C, the slices or cells were then incubated with fluorescence-conjugated secondary antibodies for 1 h. Finally, the slices or cells were incubated with DAPI for 3 min, and then, fluorescence images were captured using a Leica TCS SP8 confocal laser scanning microscope (Leica, Germany) and analyzed using Fiji ImageJ software.

2.8. Lipid droplet staining

For lipid droplet staining, cells were pretreated as described above and stained with 300 μM BODIPY 493/503 for 30 min before DAPI staining. All images were visualized under a Leica confocal microscope.

2.9. Two-color flow cytometry assay and bivariate analysis

FL-C16 (Invitrogen) was incubated with the shSelK HepG2 cells and control cells for 30min (4 °C for fatty acid binding and 37 °C for FA uptake). Then all cells were immuno-stained with anti-CD36-PE (BD) for 30 min before data acquisition using a FACScan flow cytometer. Bivariate analysis was carried out as our previously described to characterize FA binding or uptake function of CD36 [10].

Data were exported and analyzed using a previously reported bivariate spreadsheet method after excluding channels below three cell events in SPSS. These data were imported into Excel 2016, and Student's *t*-test was performed to compare the binding/uptake of fatty acid in CD36 categories displaying equivalent receptor expression between the two groups. The average level of FL-C16 binding/uptake vs. CD36 expression and the statistical results were plotted using Excel 2016.

2.10. Cell fraction assay

To separate cell fractions, 15 15-cm dishes were used for each group. The cells were first placed on ice and washed three times with precooled PBS and homogenization buffer (10 mM HEPES, pH 7.4, 150 mM sucrose, 0.5 mM DTT, and protease inhibitor cocktail (Thermo)). The washed cells were harvested with 0.8 ml homogenization buffer and homogenized with 25G needles for at least 10 times with a 1 ml syringe. After centrifugation at $2,000 \times g$ for 15 min at 4 °C, the postnuclear supernatant was collected and loaded on preformed glucose gradients. The discontinuous glucose gradients were prepared as 4 ml of 56%, 50%, 45%, 40%, 35%, 30% and 20%. After standing at room temperature for 0.5 h, the gradients were then centrifuged at 39,000 r.p.m. in a SW45Ti rotor (Beckman Instruments) for 12 h at 4 °C. A total of 15 fractions (265 μL per fraction) were obtained from top to bottom, and the bottom two fractions containing aggregated material were not analyzed. Equivalent values of each fraction were used for further analysis using western blot analysis.

2.11. Surface biotinylation

Surface biotinylation was performed on stable transfected cells. Briefly, cells were washed three times with cold PBS and treated with EZ-Link Sulfo-NHS-SS-Biotin No weight (Thermo Scientific) for 30 min shaking at 4 °C. Then, the cells were washed 3 times for 5 min with ice-cold quenching buffer (PBS containing 50 mM Glycine, pH7.4) to remove the free sulfo-NHS-SS-biotin and lysed in IP Buffer for 1 h at 4 °C. Lysate were then centrifuged for 5 min at 5000 rpm, and 30 μL supernatant were saved as input, 80 μL supernatant were incubated with 5 μL streptavidin agarose beads and rotated overnight on a wheel at 4 °C. Beads were washed with IP buffer 5 times, and the proteins were eluted from the beads by incubation in SDS sample buffer with β-mercaptoethanol for 5 min at 95 °C. The samples were separated by SDS–PAGE and analyzed by immunoblotting. Western blots were developed using the ECL protocol and imaged on a Protein Detection System (Fusion FX5). The band intensity was analyzed by densitometry software (Fiji).

2.12. Coimmunoprecipitation

For protein coimmunoprecipitations, cells were lysed for 0.5 h at 4 °C in IP buffer (0.5% NP40, 20 mM EDTA, 500 mM Tris-HCl pH 7.4, 2 mM benzamidine, 10 mM NaF, and a cocktail of protease inhibitors). Then, the cell lysates were centrifuged for 3 min at 2000 g, and the supernatants were precleared with protein A/G-magnetic beads and further incubated for 12 h at 4 °C with specified antibodies and beads. After washing 3 times, the proteins were eluted from beads by incubation in 60 μL SDS sample buffer with 10% β-mercaptoethanol for 8 min at 95 °C. Samples were tested by SDS–PAGE and analyzed by immunoblot analysis.

2.13. Acyl-RAC capture assay

S-palmitoylation of protein was assessed by Acyl-RAC assay as previously described [27] with certain modifications. For each group, 10 15-cm dishes of cells were harvested. Cells or supernatants were lysed in 400 μL buffer (25 mM HEPES, 0.5% Triton-X100, 1 mM EDTA, 25 mM NaCl, pH 7.4, and protease inhibitor cocktail), with a fraction of the cell lysate was saved as the total input. Cell lysates were incubated with 10 mM DTT at RT for 30 min. Then, 200 μL of blocking buffer (100 mM HEPES, 2.5% SDS, 1 mM EDTA, and 50 mM N-ethylmaleimide (NEM)) were added to the lysates and incubated for 4 h at 4 °C to block the free SH groups with NEM. Proteins were cold-acetone precipitated and resuspended in buffer (100 mM HEPES, 1 mM EDTA, 2.5% SDS). For treatment with hydroxylamine (NH2OH, HA) and capture by Thiopropyl Sepharose beads (GE Healthcare, USA), 2 M HA were added together with the beads (previously swelling for 10 min with sterile water) to a final concentration of 0.5 M HA and 15% (w/v) beads. 2 M NaCl was used instead of HA as a negative control. Then, the samples were incubated overnight at 4 °C on a rotating wheel. After washing 5 times, the proteins were eluted from the Sepharose beads by incubation in 80 μL SDS sample buffer with 10% β-mercaptoethanol for 8 min at 95 °C. Finally, samples were separated by SDS–PAGE and analyzed by immunoblot.

2.14. Protein half-life assay

Cells were treated with cycloheximide (100 μM) for various periods of time as described in the figure legends to block protein synthesis. Crude extracts were prepared, and the protein levels were assessed by immunoblotting.

2.15. Proximity ligation assay

The Duolink In Situ Red Starter Kit Mouse/Rabbit (DUO92101, Sigma-Aldrich, Darmstadt, Germany) was used to detect interacting proteins. For each group, cells were seeded in glass bottom cell culture dishes before the assay. Dishes were washed with PBS and fixed in 4% paraformaldehyde for 15 min. Then, the cells were blocked with Duolink Blocking Solution in a humidified chamber at 37 °C for 1 h. The primary antibodies to detect CD36 and Sec24 were added to the dishes and incubated at 4 °C for 8 h. Then, the dishes were washed with 1 × wash

buffer A and subsequently incubated with the two PLA probes (1:5 diluted in antibody diluents) for 1 h, a ligation-ligase solution for 30 min, and an amplification polymerase solution for 100 min in a humidified chamber at 37 °C. Before imaging, the dishes were washed with 1 × wash buffer B and mounted using Duolink In Situ Mounting Medium with DAPI. Fluorescence images were captured using a Leica TCS SP8 confocal laser scanning microscope (Leica, Germany).

2.16. Statistical analysis

All cell culture experiment data represent at least three independent experiments and are expressed as the means ± s.d.. The difference between two groups was statistically analyzed using Student's t-test in GraphPad Prism 8. For multiple variables analysis, we used one-way ANOVA and Tukey's multiple comparison tests. Statistical tests of significance are given in the legends of the appropriate figures.

3. Results

3.1. SelK expression is abnormally increased in the livers of mice treated with HFD

We started by studying the expression of SelK in the liver of NAFLD mouse model. Eight-week-old C57BL/6 mice were fed a high-fat diet (HFD) for 16 weeks and sacrificed for liver analysis (Fig. S1A). Hematoxylin and eosin staining and Oil Red O staining showed evident hepatocellular ballooning in the livers of the HFD group compared with the NCD group (Fig. S1B, Fig. S1C). HFD-fed mice displayed increased liver weight, intrahepatic TG content and FFA level (Fig. S1D). We detected elevated mRNA expression of SelK in vivo and *in vitro* compared with the control groups (Fig. 1A). Consistently, the Western blot analysis demonstrated that the SelK protein levels in the livers of the mice with NAFLD were higher than those in the NCD mice (Fig. 1B). Similarly, we detected an increase in the SelK protein levels in HepG2 and Huh7 cells
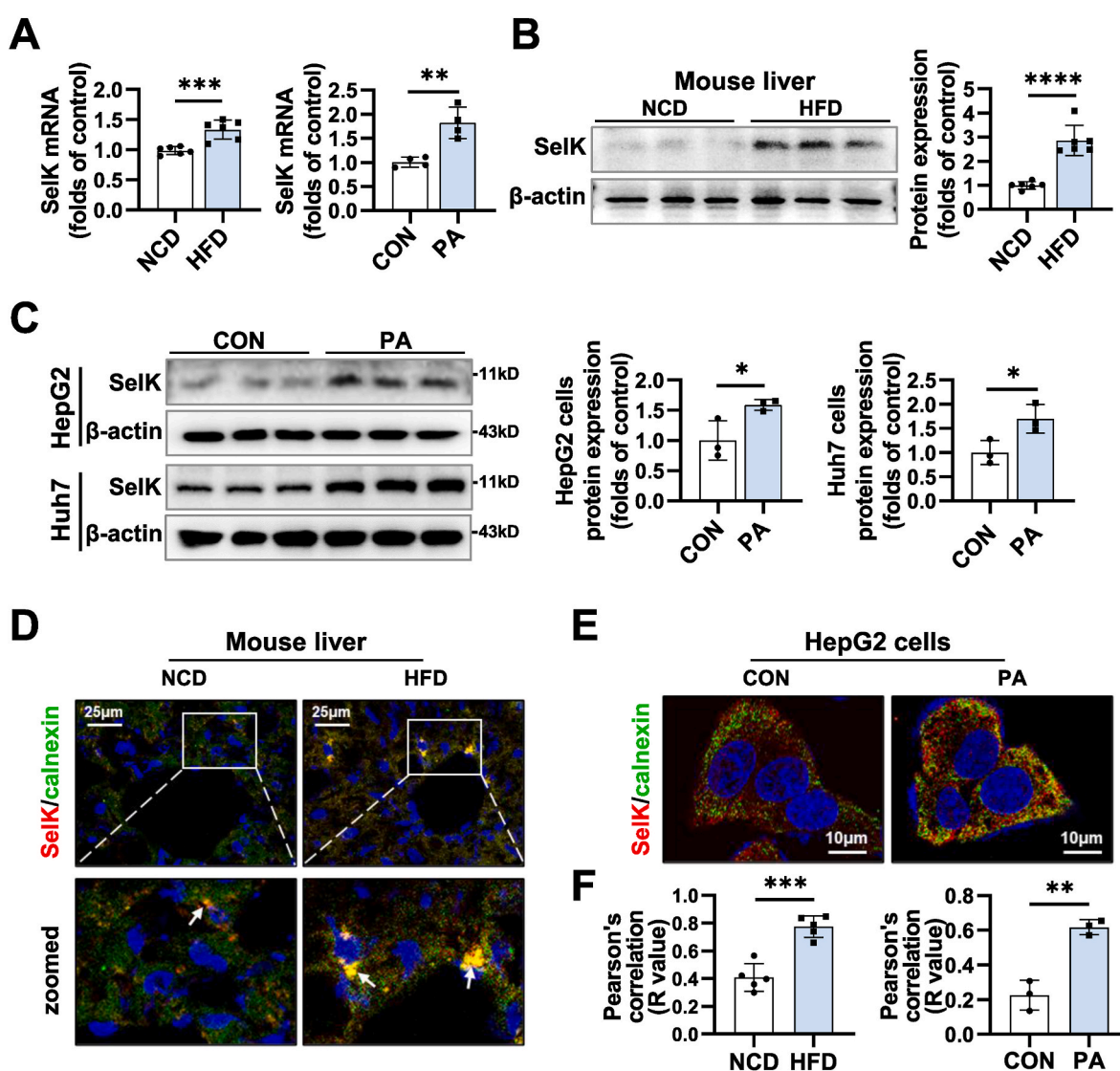

Fig. 1. SelK expression is abnormally increased in the livers of mice treated with HFD
(A) mRNA expression of SelK measured by qRT-PCR. Left panel: C57BL/6J mice high fat diet-fed (HFD) group compared to the normal chow diet-fed group (NCD). Right panel: HepG2 cells palmitic acid (160 μM) treatment group (PA) compared to the control group (CON). (B) Immunoblot analysis of SelK protein expression in mice livers (n = 6). (C) Westernblot analysis of SelK protein expression in HepG2 and Huh7 cells under PA treatment conditions, the histogram represents the expression levels. (D–F) Immunofluorescence staining of SelK (red) and ER (green) in liver tissues and HepG2 cells. The arrows indicate apparent localization of SelK in the ER. All data are shown as means ± s.d., *$P < 0.05$, **$P < 0.01$, ***$P < 0.001$, ****$P < 0.0001$. (For interpretation of the references to color in this figure legend, the reader is referred to the Web version of this article.)

under fatty acid (palmitic acid, PA) treatment conditions (Fig. 1C). Since ER is the major resident site of SelK in cells, higher ER distribution of SelK was also observed in the HFD mouse sections compared with the NCD mice and both *in vitro* (Fig. 1D–F).

3.2. The localization of CD36 is increased in the Golgi apparatus and plasma membrane under HFD or loading palmitic acid (PA) in vivo and in vitro

CD36 protein levels were increased in the livers of the mice with NAFLD than those in the NCD mice (Fig. S1E), consistent with our previous study [10]. We used immunostaining to observe the change of CD36 localization in the liver cells of the mice with NAFLD (Fig. 2A, Fig. 2B). Meaningfully, the majority of CD36 was shifted to the Golgi fractions and plasma membrane. Next, we employed a biochemical strategy to analyze ER and Golgi membrane fractions by gradient centrifugation using a previously reported method [28,29]. The bulk of the observed signal revealed that CD36 was mainly present in the ER fractions in the control groups, while most CD36 was shifted to the Golgi fractions under PA treatment conditions (Fig. 2C). These analyses indicate that subcellular translocation of CD36 were significantly changed in hepatocytes in NAFLD (see Fig. 2).
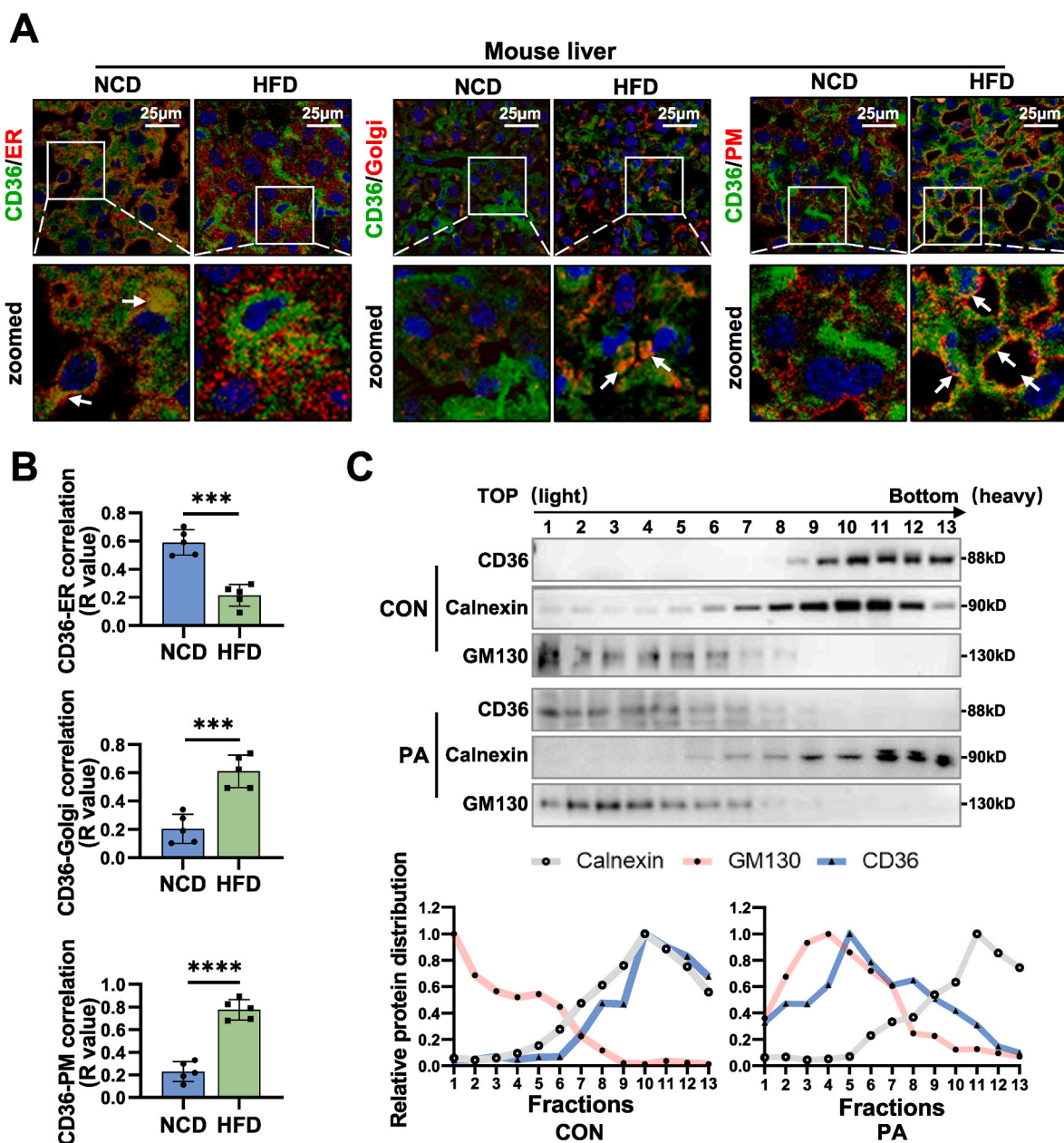

Fig. 2. Fatty acid alters subcellular localization of CD36 in hepatocytes
(A) Representative images of immunofluorescence staining of CD36 subcellular distribution in each group of mice livers (n = 5). Staining with antibodies against CD36 (green) and Calnexin (red, above), GM130 (red, middle) and Caveolin (red, below). (B) Quantification of the percentage of CD36 localized in ER-positive region (top), Golgi-positive region (middle) and Plasma Membrane -positive region (bottom), respectively. Data are shown as means ± s.d., ***P < 0.001, ****P < 0.0001. (C) Analysis of CD36 subcellular localization by fractionation. Both groups of cells were switched to serum-free medium, PA groups followed by 24h of PA treatments (160 μM), and then subjected to homogenization and cell fractionation by gradient centrifugation. The relative distribution of CD36 protein in different fractions is shown in the right panels after densitometry analysis of the blots (n = 3). (For interpretation of the references to color in this figure legend, the reader is referred to the Web version of this article.)

3.3. SelK is involved in the fatty acid uptake activity of CD36 by mediating the CD36 subcellular localization

To assess the biological function of SelK in mediating CD36 subcellular localization, immunofluorescent assay was performed to observe the distribution of CD36 in vitro. We used GM130 and TGN46 as Golgi apparatus marker, calnexin as an ER marker to observe the subcellular distribution of CD36. As shown in Fig. 3A, the knockdown of SelK resulted in a decrease of CD36 in the Golgi apparatus and promoted its retention in the ER (Fig. 3B). Cell fraction assay revealed that locally expressed CD36 was mainly present in the ER fractions in the NC group, while most CD36 was shifted to the Golgi fractions in the OE SelK group (Fig. 3C). To directly test whether SelK controls the plasma membrane localization of CD36, we used a surface biotinylation assay [30] to monitor CD36 incorporation into the plasma membrane under the effects of the Golgi-disrupting drug brefeldin A (BFA). Compared with the NC group, overexpression of SelK increased the hepatocellular membrane localization of CD36, but the BFA treatment caused a dissociation of CD36 from the plasma membrane in the OE SelK group (Fig. 3D). Furthermore, the addition of PA to shSelK-HepG2 cells failed to lead to the membrane recruitment of CD36, indicating delayed processing at the ER and trafficking through the secretory pathway of CD36 protein (Fig. 3D) (see Fig. 3).

Moreover, immunofluorescence similarly showed that CD36 was dispersed in HepG2 cells in the control groups, and principally localized on the plasma membrane in the SelK-overexpressing cells (Fig. 4A above), while failed to reach the plasma membrane and was mainly trapped inside SelK knockdown cells (Fig. 4A below). We next examined whether SelK is required for the physiological fatty acid binding/uptake function of CD36. BODIPY staining indicated that the overexpression of SelK elevated the uptake of PA (Fig. 4B, above), while the knockdown of SelK reduced contrarily (Fig. 4B, below), indicating that SelK is required for the fatty acid uptake activity of CD36. To directly detect the effects of SelK on the activity of CD36 in HepG2 cells, a two-color flow cytometry assay was used, and the data were exported and analyzed using a bivariate analysis. As shown in Fig. 4C, inhibition of SelK significantly bring down the FL-16 binding (Fig. 4C, left) and uptake (Fig. 4C, right) in a manner dependent on the surface expression of CD36. Together, these data suggest that SelK is involved in the fatty acid uptake activity of CD36 by mediating the subcellular localization of CD36 (see Fig. 4).

3.4. Loss of palmitoylation inhibits the loading of CD36 into COPII vesicles

In eukaryotic cells, proteins that are transported to several intracellular organelles or the plasma membrane are first synthesized and processed in the ER [31]. The secretory pathway comprises structurally distinct organelles and membrane-bound transport intermediates that facilitate transport between them (Fig. S2A). Coat protein complex II (COPII) comprises a set of highly conserved proteins responsible for creating small membrane vesicles that originate from the ER [32,33]. COPII consists of the following five cytosolic proteins: Sar1, Sec23, Sec24, Sec13 and Sec31. In cells, Sec23 and Sec24 are found in tight heterodimers that form the inner COPII coat, whereas Sec13 and Sec31 form the outer COPII coat [34]. Sar1 and these two types of stable complexes are sequentially recruited to the ER membrane and work together to create a complete COPII vesicle [35,36]. The Sec23–Sec24 complex arrives at the site by right of the direct interaction between Sar1 and Sec23 [37]. Sec24 is deemed the primary subunit responsible for binding cargo proteins at the ER and centralizing these proteins into the forming vesicles [38].

Our previous study demonstrated that fatty acid increased CD36 palmitoylation and promoted CD36 localization on the hepatocellular plasma membrane [10]. We repeated these analyses (Figs. S2B–D) and observed a similar induction of CD36 palmitoylation in SelK overexpressing HepG2 cells, while the knockdown of SelK on the contrary

(Fig. S2E). Therefore, we tested whether palmitoylation affects the loading of CD36 into COPII vesicles.

To examine the effect of palmitoylation on the integration of CD36 into COPII, we generated a mutant that had the four palmitoylation sites mutated from Cys to Ala or Ser, designated AA-SS, which was no longer palmitoylated. Adeno-associated virus AAV2/8 vectors containing wild-type CD36 (WT-CD36) or palmitoylation site-mutated CD36 (AA-SS) were injected into CD36-KO mice via the tail vein, and the mice maintained on a HFD for 8 weeks (Fig. 5A). Hepatic steatosis was decreased in the CD36-KO-AA-SS mice compared with that in the CD36-KO-WT-CD36 mice (Fig. 5B).

The immunofluorescent staining showed augmented colocalization between CD36 and Sec24 in the NAFLD mouse liver slides (Fig. 5C, G left). Strikingly, the mutation of palmitoylation site decreased the association between CD36 and Sec24 in the CD36-KO-AA-SS mice compared with that in the WT-CD36 mice (Fig. 5D, G right). Next, we performed an immunoprecipitation assay to directly examine CD36 combination with Sec24 to confirm CD36 packaging into COPII vesicles. Consistently, a high-fat diet increased the amounts of Sec24 found in CD36 immunoprecipitation assay from mouse livers (Fig. 5E, H left), while there was a decrease in the association between CD36 and Sec24 in the AA-SS mice compared with that in the WT-CD36 mice (Fig. 5F, H right). These data suggest that loss of palmitoylation inhibits the loading of CD36 into COPII vesicles (see Fig. 5).

3.5. Sar1B, an initiator of COPII vesicle formation, is increased under HFD or loading palmitic acid (PA) in vivo and in vitro

The immunostaining pattern in HepG2 cells exhibited a colocalization of Sec24 and CD36, indicating that PA induced CD36 to be enriched within COPII vesicles (Fig. 6A, Fig. 6E left). In contrast, in the transfected HepG2 cells, the AA-SS mutant exhibited reduced colocalization with Sec24, suggesting that palmitoylation is required for the integration of CD36 into COPII (Fig. 6B, E right) in vitro. Additionally, immunoprecipitation assay from PA treated HepG2 cells (Fig. 6C, F left) suggested an increased CD36-Sec24 association compared with that in the control groups, which is consistent with mouse livers. While, the immunoprecipitation assay showed a decrease in the association between CD36 and Sec24 in AA-SS mutant HepG2 cells (Fig. 6D, F right). To further confirm the change of CD36-Sec24 association, we used an in-situ proximity ligation assay (PLA). Detection of only the CD36 primary antibody served as a negative control. In this approach, PA treatment increased the puncta of positive fluorescence signals in HepG2 cells (Fig. S3A) and CD36-WT-HepG2 cells exhibited stronger positive fluorescence signals than CD36-AASS-HepG2 cells (Fig. S3B) .

After determining that a deficiency of palmitoylation markedly decreased the association between CD36 and Sec24 in vivo and in vitro, we sought to investigate which component(s) of COPII was changed during this procedure. Based on the consistent results above, we studied the expression pattern of COPII components in mouse livers and HepG2 cells by a Western blot analysis. As shown in Fig. 6G, the protein of Sar1B is expressed at relatively high levels in HFD-fed mice and PA-incubated HepG2 cells (Fig. 6H). The presence of Sar1B stimulates the recruitment of the inner coat components Sec23 and Sec24, which are responsible for capturing cargo proteins into nascent COPII vesicles [37, 39]. Therefore, the elevation in Sar1B indicates an inordinate elaboration of COPII vesicle transport under fatty acid treatment (see Fig. 6).

3.6. SelK increases the activation of Sar1B and triggers nascent COPII vesicles formation

To better understand the abnormal expression of Sar1B, we considered that SelK is involved in the regulation of ER associated protein homeostasis [40,41]. The most important and meaningful is that overexpression of SelK increased the protein level of Sar1B, and in contrast, knockdown of SelK reduced it (Fig. 7A, Fig. 7B), with no change at the
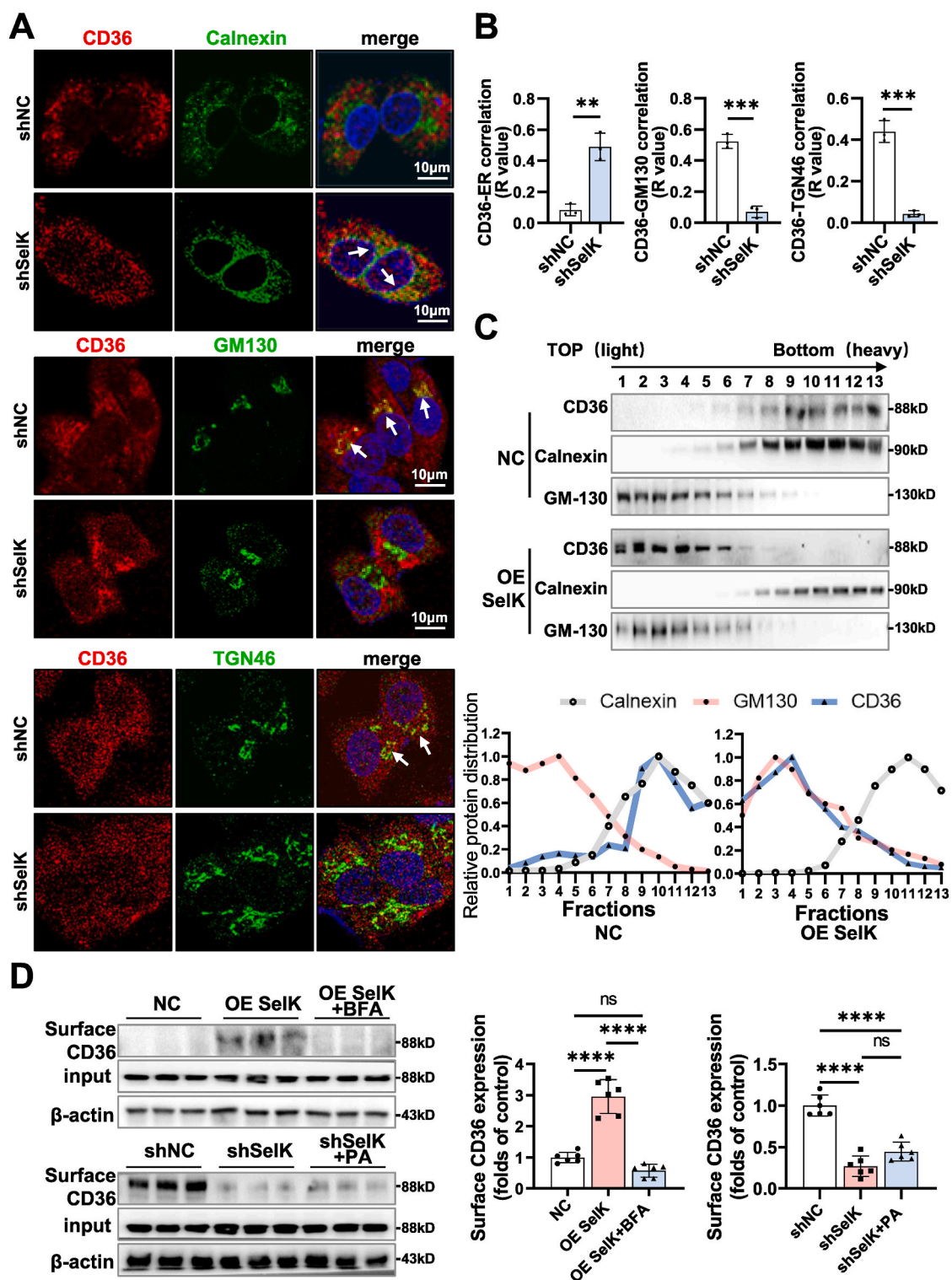
Fig. 3. SelK mediates the subcellular localization of CD36

On Day 0, HepG2 cells were set up in 60-mm dishes. On Day 2, cells were transfected with lentivirus expressing SelK (OE SelK) or knockdown SelK (shSelK) (MOI = 10). Lentivirus vectors expressing negative controls (NC or shNC) respectively. (A) Knockdown of SelK reduced the endogenous CD36 that are enriched in the Golgi apparatus. At 36 h after the transfection, the cells were switched to serum-free medium for 12 h, followed by 24 h of PA treatment. Representative dual-immunoflorescent staining image of CD36 (green) and Golgi apparatus (left, red) or ER (right, red) in shSelK HepG2 cells. (B) The histogram of (A), data are shown as means ± s.d., **$P < 0.01$, ***$P < 0.001$. (C) Overexpression of SelK enhanced endogenous CD36 in the Golgi apparatus. Analysis of CD36 subcellular localization by fractionation. SelK gene were transfected into HepG2 cells. Cells were switched to serum-free medium for 12 h followed by 24 h of PA treatments, and then subjected to homogenization and cell fractionation by gradient centrifugation. The relative distribution of CD36 protein in different fractions is shown in the following panel after densitometry analysis of the blots (n = 3). (D) Cells were treated with 5 μg/ml BFA or 160 μM PA for 16 h before harvested for surface biotinylation assay as described in *Materials and method*. Equal volume of input and eluted fraction for each treatment was loaded on an SDS–PAGE gel and immunoblotted with β-actin antibody (n = 6). Data are shown as means ± s.d., ****$P < 0.0001$, $^{ns}P > 0.05$. (For interpretation of the references to color in this figure legend, the reader is referred to the Web version of this article.)
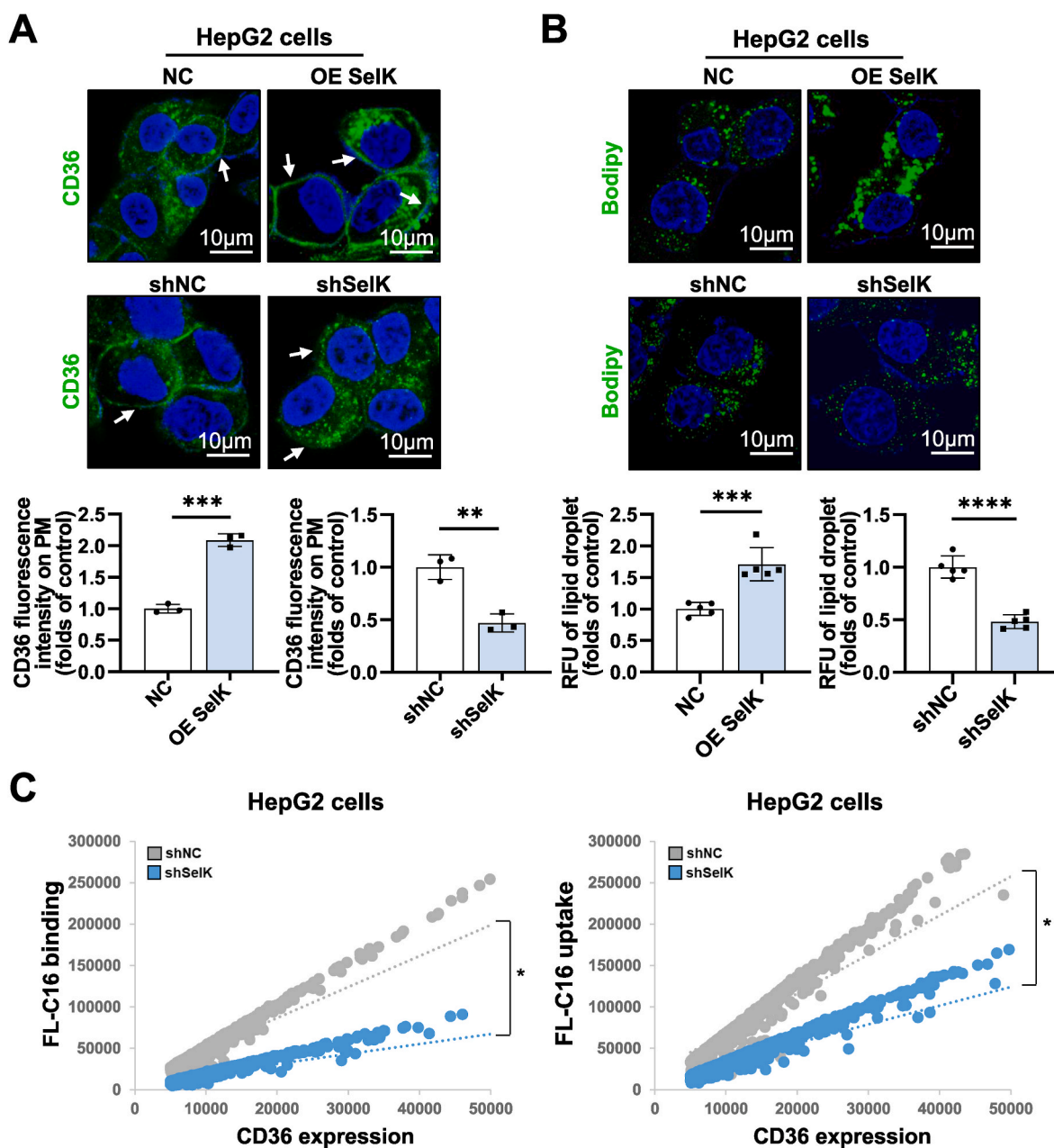
Fig. 4. SelK is involved in the fatty acid uptake activity of CD36

(A) SelK is required for the plasma membrane localization of CD36. Representative confocal microscopy images of CD36 induced by overexpressed SelK or knockdown SelK in HepG2 cells. Fluorescence intensity of CD36 on plasma membrane (PM). Data are shown as means ± s.d., **$P < 0.01$, ***$P < 0.001$. (B) BODIPY staining in HepG2 cells transfected with SelK lentivirus (above) and shSelK lentivirus (below) (n = 5). Data are shown as means ± s.d., ***$P < 0.001$, ****$P < 0.0001$. (C) Knockdown of SelK reduced fatty acid (FA) transport via CD36. On Day 4, cells were incubated with FL-C16 for 30 min at 4 °C (above) and 37 °C (below) and labeled with PE-CD36, followed by a bivariate FACS analysis. Low-capability of long-chain fatty acid (LCFA) binding in SelK-knockdown-HepG2 cells (above). Low-capability of LCFA uptake in SelK-knockdown-HepG2 cells (below). Independently repeated for 5 times.

genetic level (Fig. 7C). We therefore speculated that SelK influenced the degradation of Sar1B in ER. The protein synthesis inhibitor cyclohexi-mide (CHX) was used to block the supply of newly synthesized Sar1B in the SelK overexpression or knockdown groups. As shown in Fig. 7D, CHX treatment alone caused a prolong of Sar1B in the OE SelK group compared with NC group, indicating an apparent extension of half-life for 10 h. While a decay of Sar1B observed in the shSelK group was ≈3 h, compared with the shNC group.

Importantly, COPII vesicle biogenesis is initiated by the activation of a Sar1B protein through Sec12, a guanine nucleotide exchange factor [42,43]. Next, we examined whether the interaction between Sar1B and Sec12 was changed under SelK intervention. Immunoprecipitation assay

demonstrated the SelK knockdown resulted in a greater reduction in Sec12-Sar1B complex expression compared with that in the shNC group (Fig. 7E). Thus, the induction of the interaction between Sec12 and Sar1B is partially due to the abnormal increase in SelK expression in HepG2 cells (see Fig. 7).

3.7. SelK accelerates the palmitoylated-CD36 integration into COPII vesicles

To further verify the effect of SelK on mediating the loading of CD36 into COPII vesicles, we again examined the combination between Sec24 and cargo CD36. Compared with the NC group, overexpression of SelK
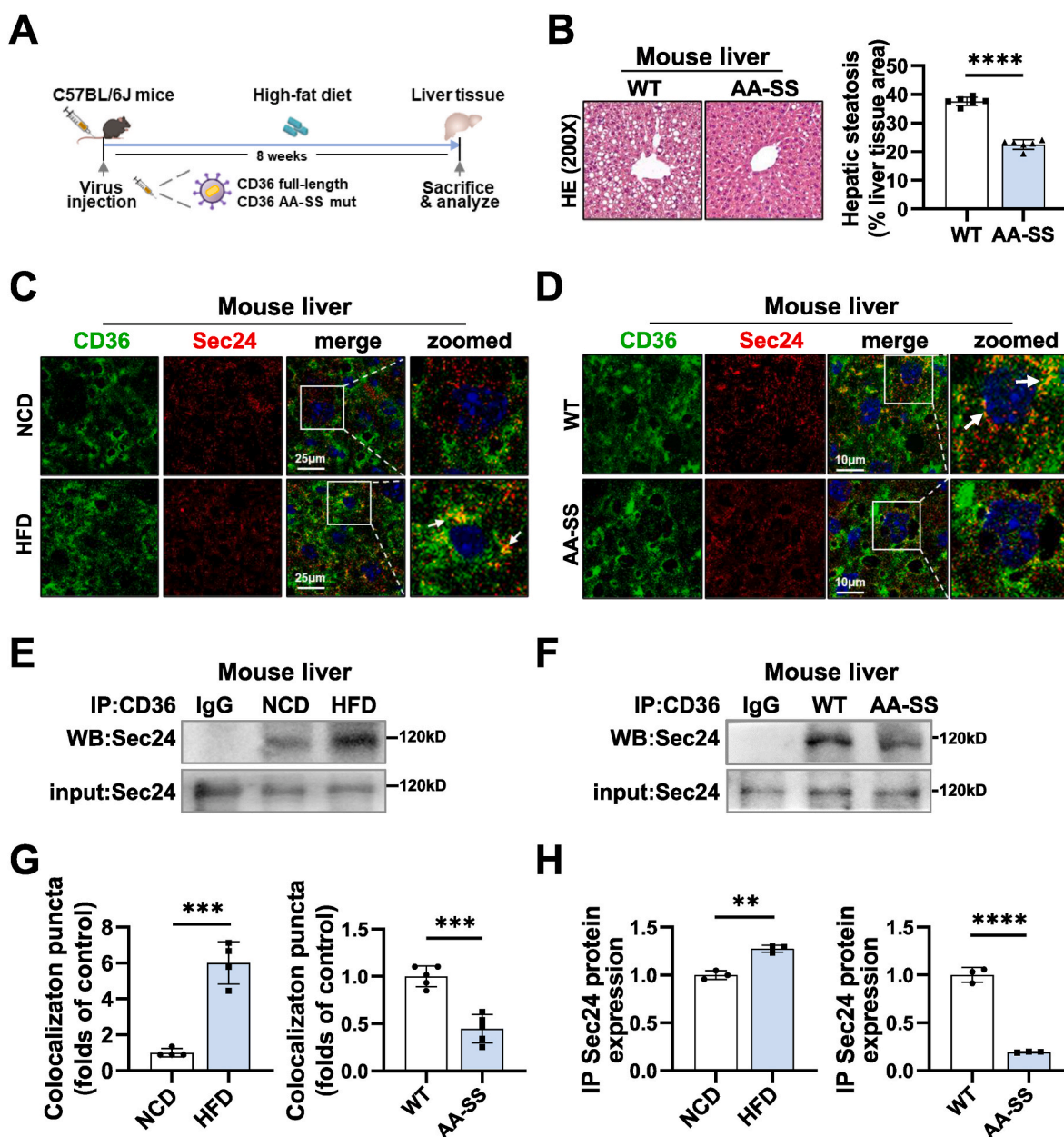
Fig. 5. Loss of palmitoylation inhibits the loading of CD36 into COPII vesicles

(A) Schematic outline of experimental approaches and analyses. Adeno-associated virus AAV2/8 vectors (AAV) containing wild-type CD36 (WT) or palmitoylation site-mutated CD36 (AA-SS) were injected into CD36-KO mice via the tail vein, and the mice maintained on a HFD for 8 weeks. (B) Inhibition of CD36 palmitoylation ameliorated hepatic steatosis in mice. Histopathological examination of mouse livers. Representative pictures of HE staining (n = 6). (C and D) Palmitoylation enriches CD36 into COPII via interacting with Sec24. Dual-immunoflorescent staining of CD36 and Sec24 on mice livers (n ≥ 4). (E and F) Loss of palmitoylation inhibits the combination of CD36 with Sec24. Co-immunoprecipitations of CD36 and Sec24 in livers and representative results. (G) Pearson's correlation of CD36 and Sec24. (H) Histograms represents the combination levels of CD36 and Sec24. All data are shown as means ± s.d., **$P < 0.01$, ***$P < 0.001$, ****$P < 0.0001$.

stimulated the Sec24-CD36 interaction, while SelK knockdown led to a significant reduction (Fig. 8A). The reduced combination between CD36 and Sec24 in the shSelK cells indicated that depressed Sar1B caused a decrease in cargo CD36 wrapped into COPII (Fig. 8B).

Bearing in mind that SelK has been reported for its role in mediating palmitoylation by interacting with DHHC6 palmitoyltransferase through Src-homology 3 (SH3) binding domain [24]. We generated two separate lentiviral plasmids expressing the full-length SelK (SelK Full-length) and truncated SH3 binding domain (SH3 BD TRUNC), hence the binding ability was lost in cells transfected with SelK SH3 BD TRUNC lentivirus. Acyl-RAC assay and surface biotinylation assay were performed. As shown in Fig. 8C, the palmitoylation of CD36 was upregulated in the SelK Full-length groups, while the SH3 BD TRUNC groups

were no longer palmitoylated (Fig. 8C, F). Similarly, the surface content of CD36 was increased in the SelK Full-length groups, and the combination domain truncation caused a dissociation of CD36 from the plasma membrane (Fig. 8D, G). Furthermore, we observed the subcellular localization of CD36 in the SelK Full-length and SH3 BD TRUNC-HepG2 cells. The truncation of SH3 binding domain resulted in a decrease of CD36 in the Golgi apparatus and promoted its retention in the ER (Fig. 8E, H), which was consistent with the SelK knockdown (Fig. 3A). Thus, through increasing the stability of mature Sar1B protein, SelK increased the levels of Sar1B expression and palmitoylated CD36 integrated into COPII vesicles, exceptionally.
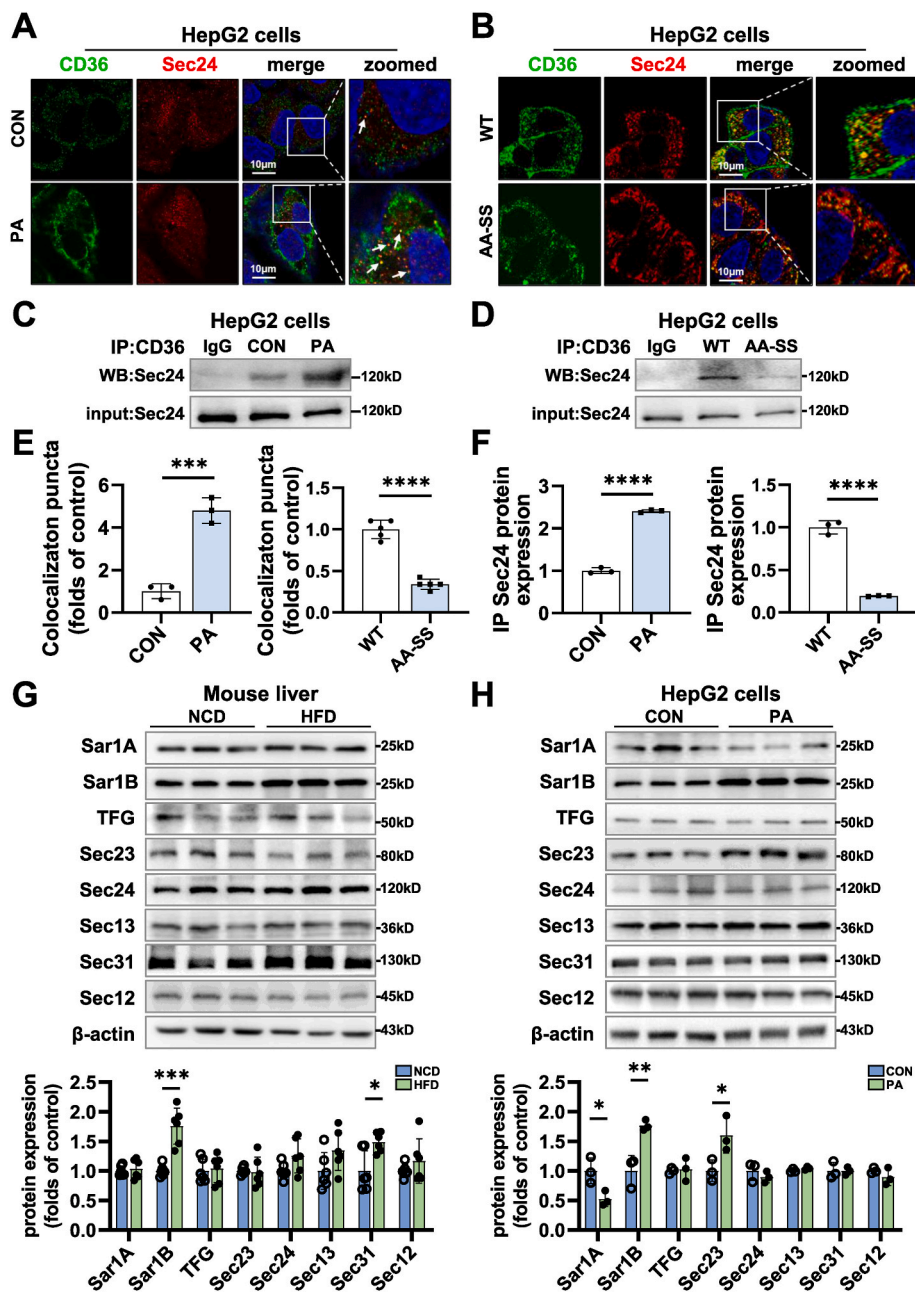
Fig. 6. HFD stimulates Sar1B which initiates the recruitment of nascent COPII vesicles

(A and B) Dual-immunoflorescent staining of CD36 (green) and Sec24 (red) in HepG2 cells. HepG2 cells were pretreated with 160 μM PA for 16 h (A), or pre-infected with lentivirus expressing CD36-AA-SS for 48 h (B). (C and D) Co-immunoprecipitations of CD36 and Sec24 in HepG2 cells (n = 3). (E) Pearson's correlation of CD36 and Sec24. (F) Quantification of coimmunoprecipitation results of the interaction between CD36 and Sec24 in cells from the different groups. (G) Protein levels of COPII components in liver tissues. (H) HepG2 cells were incubated with serum-free medium for 12 h, followed by 24 h of 160 μM PA treatments. Protein levels of COPII components in HepG2 cells. All data are shown as means ± s.d., *$P < 0.05$, **$P < 0.01$, ***$P < 0.001$, ****$P < 0.0001$. (For interpretation of the references to color in this figure legend, the reader is referred to the Web version of this article.)

3.8. Intervention of SelK SH3 binding domain protects mice from NAFLD via regulating CD36 subcelluar trafficking

To further identify the role of the SelK in NAFLD, AAV2/8 vectors containing SelK full length (WT) or SH3 binding domain truncated SelK (SH3 BD TRUNC) were injected into C57BL/6J wild-type mice via the tail vein, and the mice were maintained on a HFD for 8 weeks (Fig. S4A). We found that hepatic steatosis and lipid accumulation were reduced in the SH3 BD TRUNC mice compared with those in the WT mice (Fig. 9A, Fig. 9B). The liver weight, intrahepatic TG content and FFA level showed a consistent reduction (Fig. S4B). These results support that inhibiting the participation of SelK in mediating palmitoylation achieved an improvement in NAFLD.

Next, we tested the CD36 distribution in mouse liver tissues. Consistent with our fractionation results (Fig. 3C), CD36 was mainly colocalized with the ER marker calnexin in control group (Fig. 9C above, Fig. 9D left). The transfection of WT-SelK led to an increase in CD36

mobilization to the Golgi apparatus and plasma membrane (Fig. 9C middle and bottom, Fig. 9D middle and right). In the SH3 BD TRUNC mice, CD36 appeared to have a preference for ER and a reduction in Golgi apparatus and plasma membrane in contrast to the WT-SelK mice. Furthermore, the combination of CD36 and Sec24 was decreased in the SH3 BD TRUNC group (Fig. 9E, G left). The plasma membrane expression of CD36 protein was obviously increased in the livers of the mice transfected with WT-SelK, and this increase could be inhibited by truncating the SH3 binding domain (Fig. 9F and G right).

4. Discussion

Selenoproteins are responsible for the biological actions of the trace element selenium (Se) [44]. The well-characterized members include iodothyronine deiodinase (Dio), glutathione peroxidases (GPx), methionine sulfoxide reductase (Msr), thioredoxin reductases (TrxR), and especially ER selenoproteins (SelS, SelK, SelM, SelN and Sel15) [45–47].
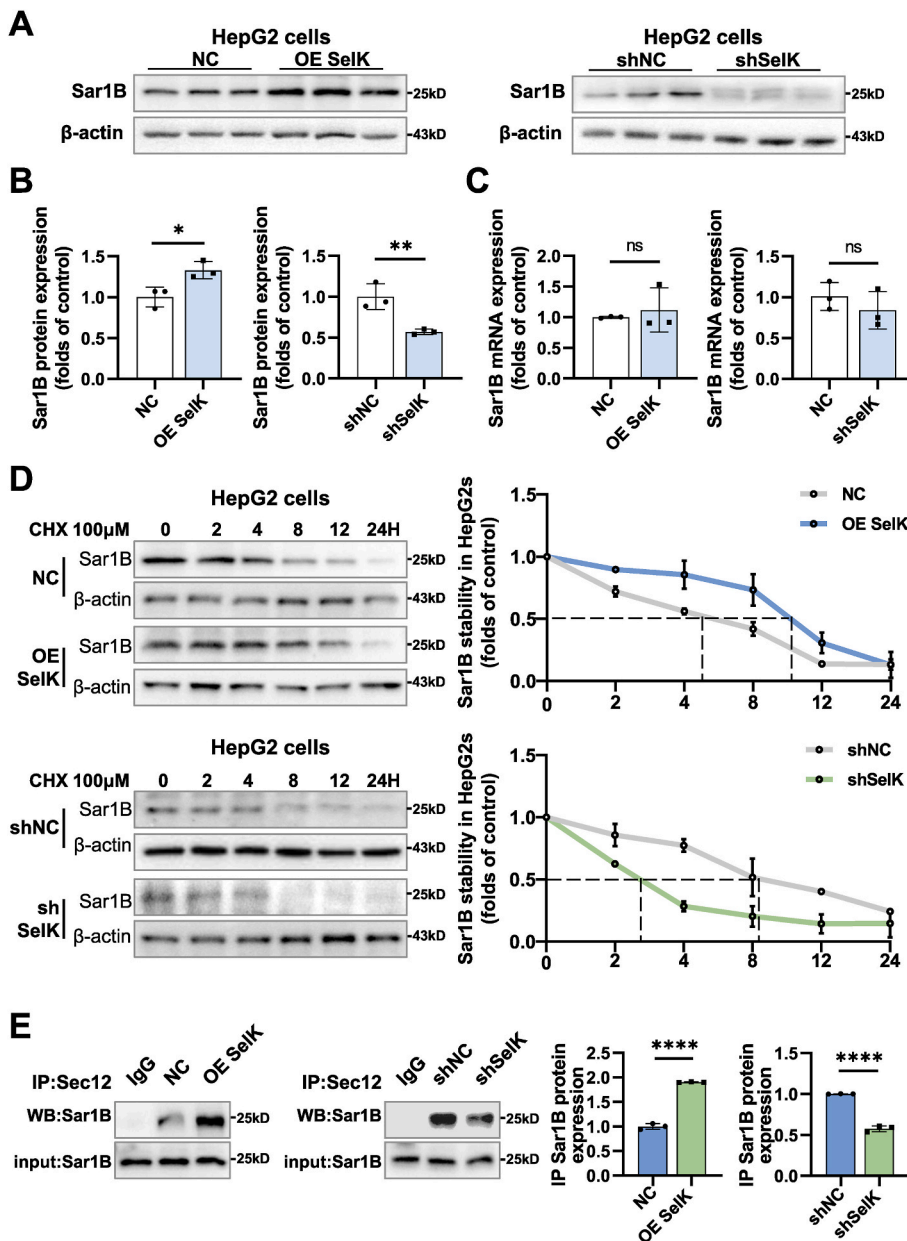
Fig. 7. SelK increases the activation of Sar1B and triggers nascent COPII vesicles formation

(A and B) On Day 0, HepG2 cells were infected with lentivirus expressing SelK or SelK-knockdown were set up as in Fig. 3. On Day 2, cells were harvested, Sar1B expression were analyzed by Western blot. (C) mRNA expression of Sar1B in HepG2 cells transduced with scrambled or SelK expressing lentivirus (left)/ SelK shRNAs (right) as measured by qRT-PCR. (D) SelK prolongs the life-span of Sar1B. On Day 0, SelK overexpressing and knockdown HepG2 cells were set up as in (A). On Day 2, cells were treated with 100 mg/mL CHX for the indicated time. Cells were harvested, Sar1B degradation were analyzed by Western blot (n = 3). (E) SelK promotes Sec12 - induced activation of Sar1B. HepG2 cells were set up as in (A). Co-immunoprecipitations of Sec12 - Sar1B in HepG2 cells (n = 3). All data are shown as means ± s.d., *$P < 0.05$, **$P < 0.01$, ****$P < 0.0001$, ns$P > 0.05$.

The discovery of disease-associated polymorphisms in selenoprotein genes has drawn attention to the relevance of selenoproteins to health in past decade [48]. The immune system relies on adequate dietary selenium intake and this nutrient exerts its biological effects mostly through its incorporation into selenoproteins [49]. Conflicting data link metabolic diseases, such as NAFLD and type-2 diabetes, with Se and selenoproteins [50,51]. Our findings innovatively extended the studies of selenoproteins into lipid metabolic researches.

Growing evidence emphasizes possible disadvantageous cardiometabolic effects of high Se exposure, specifically dyslipidemia and type 2 diabetes [52,53]. Biologically, Se can also contribute to the development of NAFLD. Both excess Se and Se deficiency may alter hepatic metabolism in animals [54,55]. Se treatment impairs insulin responsiveness and disrupts lipid profiles in animal models despite its insulin-like and antioxidant properties [56–59]. Furthermore, randomized clinical trials and observational studies have explored high Se may be linked to an increased risk of NAFLD [60–62]. Interestingly, we preliminarily analyzed the database of a transcriptome profile about fatty liver [63] and also found that the *SelK* gene had higher expression

in steatosis and NASH groups than in healthy normal-weight controls. Therefore, this study aimed to uncover a central role of the selenoprotein family member SelK in the regulation of hepatic lipid metabolic homeostasis independent of its reported redox equilibrium and modulation of calcium flux function.

SelK, a small molecular selenoprotein (~11 kDa) located in the ER membrane, is regulated by dietary selenium and widely expressed in numerous tissues in mammalian [64]. In brain and skeletal muscle, SelK plays crucial roles in protecting neurons and skeletal muscle from apoptosis through the modulation of ER stress and against oxidative stress [65,66]. Besides, SelK knockout mice exhibit deficient calcium flux in immune cells and impaired immune responses. In cancers like melanoma, it has been found an apparent dependence on SelK function for tumor growth and metastasis [67]. Although SelK is closely related to immunity, cancer and development, but its function in regulating the progression of NAFLD has not been reported. Our study implicates a striking increase of SelK in NAFLD mouse livers. Based on our previous study that the increased localization of CD36 on hepatocyte plasma membranes may represent a key feature in the development of NAFLD
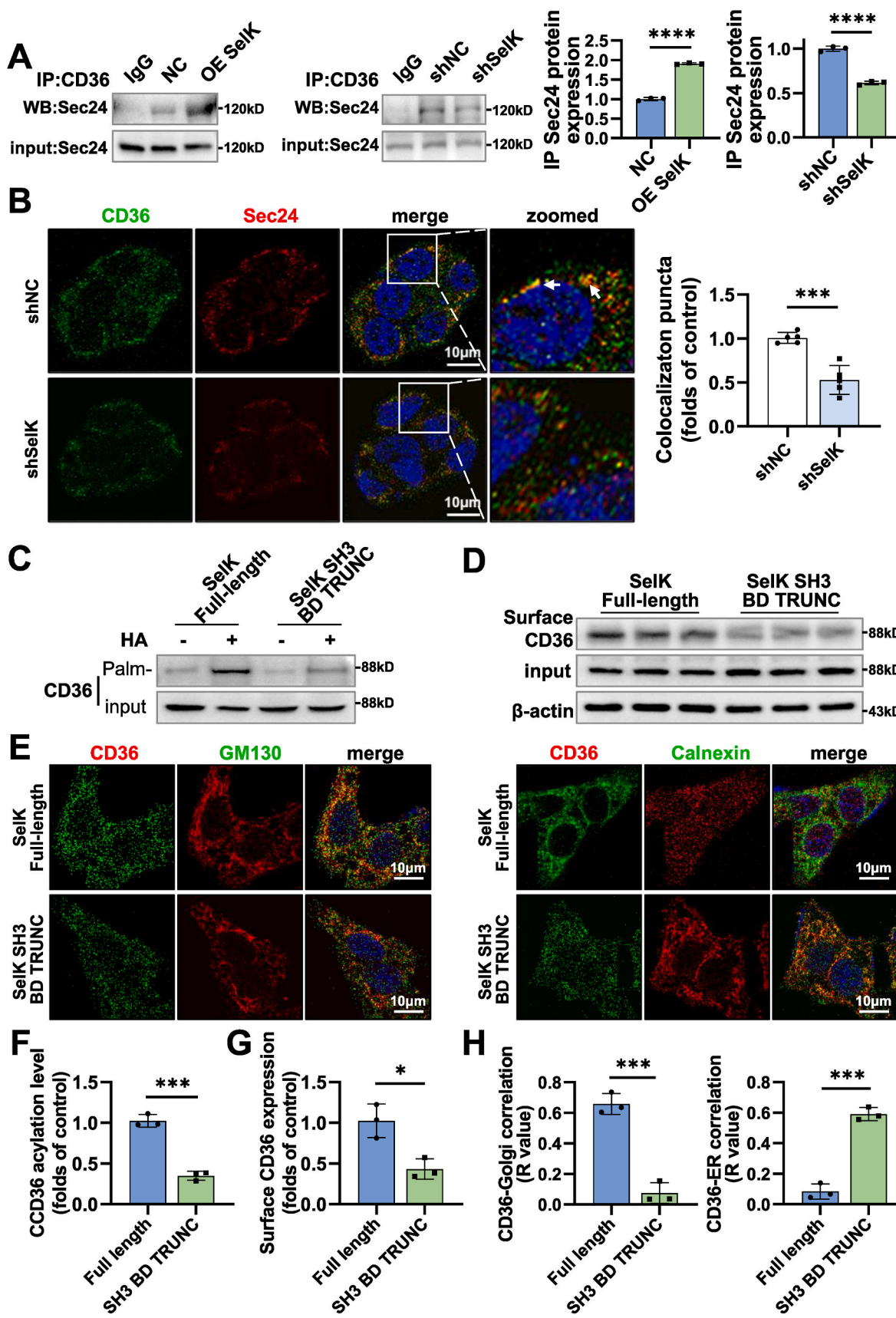
(caption on next page)

Fig. 8. SelK accelerates the cargo CD36 integration into COPII vesicles

(A and B) HepG2 cells were infected with lentivirus expressing SelK or SelK-knockdown were set up as in Fig. 3. (A) Co-immunoprecipitions of CD36 - Sec24 in HepG2 cells (n = 3). (B) Dual-immunoflorescent staining of CD36 (green) and Sec24 (red) in cells (n = 5). (C–E) HepG2 cells were transfected with wild-type SelK lentivirus (SelK Full-length) or SelK lacking the SH3-binding domain lentivirus (SelK SH3BD TRUNC). (C) Cells were harvested and subjected to an Acyl-RAC assay (n = 3). Input and eluted fractions were separated on SDS gels and subjected to immunoblotting with anti-CD36 antibodies. (D) Cells were harvested and subjected to surface biotinylation. Equal volume of input and eluted fraction for each treatment was loaded on an SDS-PAGE gel and immunoblotted with β-actin antibody. (E) Deletion of the SH3 binding region in SelK decreased the endogenous CD36 that are enriched in the Golgi apparatus. On Day 0, HepG2 cells transduced with SelK full-length or SelK SH3BD truncated lentivirus were set up as described in (A). On Day 2, cells were incubated with serum-free medium for 12 h followed by 24 h of 160 μM PA treatments. On Day 3, cells were subjected to immunofluorescence assay using the anti-CD36 (green) and anti-GM130 (red, left) or anti-Calnexin (red, right) antibodies. (F) Quantification of CD36 palmitoylation level in cells. (G) Quantification of surface biotinylation results of the CD36 in cells. (H) Pearson's correlation of CD36 and Golgi apparatus (left) or ER (right). All data are shown as means ± s.d., *$P < 0.05$, ***$P < 0.001$, ****$P < 0.0001$. (For interpretation of the references to color in this figure legend, the reader is referred to the Web version of this article.)
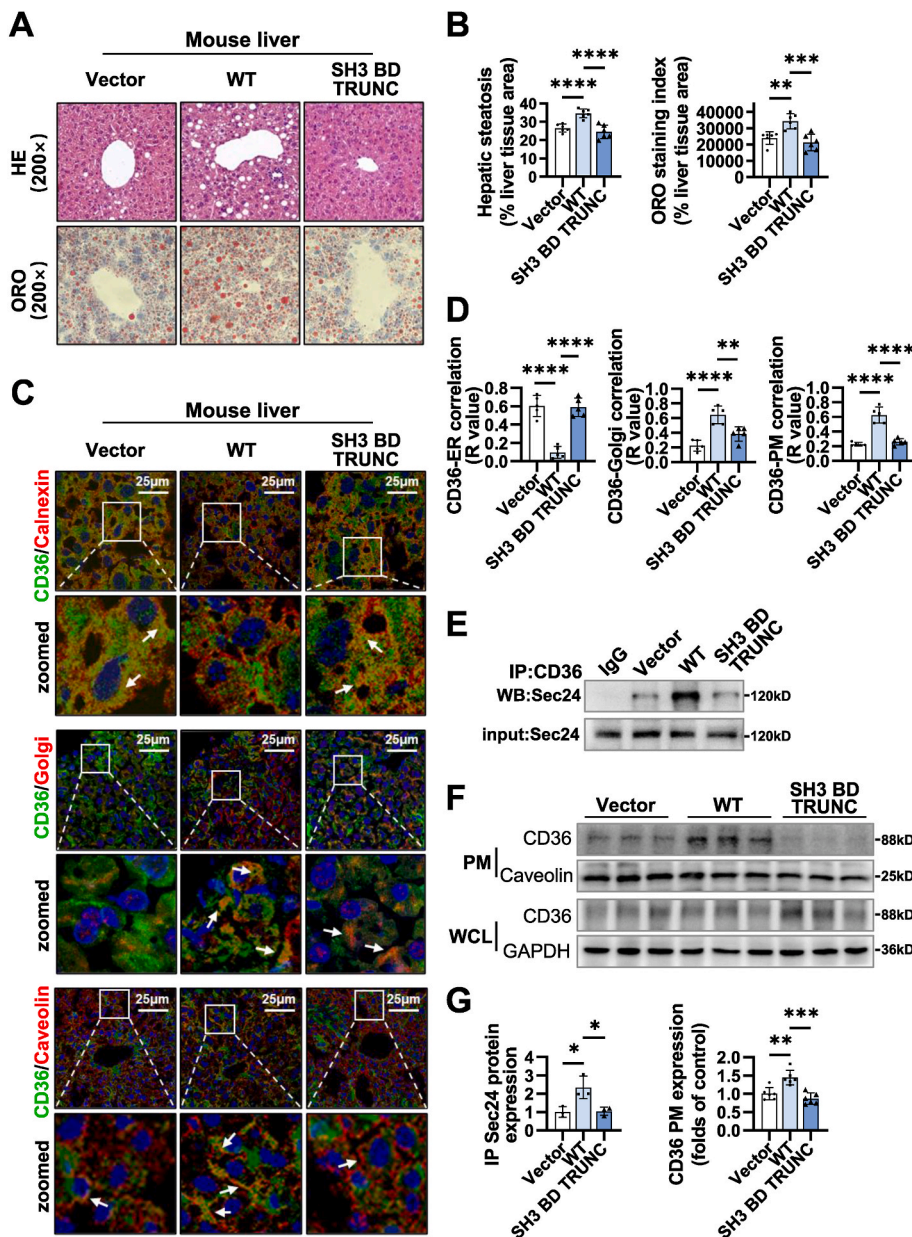

Fig. 9. Inhibition of SelK SH3 domain protects mice from NAFLD

(A) Histopathological examination of AAV injected C57BL/6 J livers. Representative pictures of HE staining (above) and ORO staining (below) in liver sections from mice (n = 6). (B) Representative images of immunofluorescence staining of CD36 subcellular distribution in each group of mice livers (n = 5). Staining with antibodies against CD36 (green) and Calnexin (red, above), GM130 (red, middle) and Caveolin (red, below). (C) Histograms represent H&E and Oil Red O staining of liver tissues. (D) Quantification of the percentage of CD36 localized in ER-positive region (left), Golgi-positive region (middle) and Plasma Membrane-positive region (right), respectively. (E) Co-immunoprecipitions of Sec24 and CD36 in mice livers. (F) Expression of CD36 in plasma membrane and total proteins extracted from mice livers (n = 6). (G) Quantification of CD36-Sec24 combination level (left) and plasma membrane expression level (right) of CD36 in mice livers from the different groups. All data are shown as means ± s.d., *$P < 0.05$, **$P < 0.01$, ***$P < 0.001$, ****$P < 0.0001$. (For interpretation of the references to color in this figure legend, the reader is referred to the Web version of this article.)

[10], we first found that the activation of SelK induced the CD36 subcellular trafficking and increased the plasma membrane distribution of CD36 by accelerating its subcellular trafficking in hepatocytes. Beside our findings, the role of SelK in progression of NAFLD is still in need for further study. Considering the function of SelK in modulation of ER stress and oxidative stress in other tissues, we speculate that the physiological levels of SelK in hepatocytes may be important to keep a balance of reactive oxygen species (ROS), lipid metabolism, and the inflammatory response. Therefore, maintaining a balance of hepatic SelK and CD36 subcellular trafficking could be a potential new therapeutic strategy for the prevention of NAFLD development. In addition, we only used male mice in the experimental design, resulting in some

weaknesses in this study. Recent studies have found that age upregulated SelK in the kidneys of female mice, while only in testes of males [68]. Although it seems that SelK appears no change in both male and female mice livers under the age of 18 months, whether sex is a biological variable in liver tissues still worthy of consideration.

Each mammalian cell type contains a specific suite of trafficking protein cargos referred to as the trafficking machinery to provide both this unidirectionality of subcellular trafficking and the appropriate sorting mechanisms. The cellular fatty-acid uptake rate is governed primarily by the presence of CD36 at the cell surface, which is regulated by the subcellular vesicular recycling of CD36 from endosomes to the sarcolemma in cardiac myocytes [69,70]. Unlike heart, hepatic CD36 expression is normally lower, but its expression and membrane distribution are specifically increased under steatosis stimulus, which appear more meaningful in NAFLD pathogenesis. Thus, the subcellular trafficking mechanisms of CD36 have not yet been uncovered in hepatocytes. At present, the compartments of the secretory pathway beginning with the site of cargo synthesis include the ER, ERES, ERGIC, Golgi complex, and trans-Golgi network [32]. This led to a model in which the biosynthetic trafficking pathway (or secretory pathway) is divided into two sections. In the early pathway common to most secreted proteins, COPII vesicles transport newly synthesized protein cargos (and membrane lipids) from the ER to the Golgi apparatus, whereas COPI vesicles mediate transport back from the Golgi apparatus to the ER and within the Golgi stacks [71]. Remarkably, our results show that SelK, as an ER resident protein, concentrates the CD36 membrane cargo into forming COPII vesicles by regulating its combination with Sec24 and accelerates the ER-Golgi transfer of CD36 by facilitating the assembly of COPII vesicles through mediating the stability of Sar1B (Fig. 10).

Posttranslational modification, such as palmitoylation and glycosylation, provides an important mechanism for regulating protein subcellular localization [72,73]. Among the rest, palmitoylation has emerged as an important posttranslational modification that regulates the expression, localization, and function of a wide variety of proteins [74–76]. Although palmitoylation is well known to be important for membrane distribution of several proteins [14,77–79], it should be noted that we found that palmitoylation is required for the ER-Golgi transport of CD36 in hepatocytes. This study demonstrates more deeply that palmitoylation could potentially ensure CD36 subcellular trafficking, therefore facilitating CD36 membrane targeting and biological function. CD36 mutant, that had the four palmitoylation sites mutated from Cys to Ala or Ser, designated AA-SS, was no longer palmitoylated. The mutation of palmitoylation sites markedly decreased the association between CD36 and COPII vesicles and alleviated the subcellular trafficking of CD36.

Palmitoylation can be catalyzed by palmitoyltransferases, also called DHHC, because of their conserved Asp-His-His-Cys sequence and can be removed by acyl protein thioesterases [80–82]. Recent studies have found that SelK as a cofactor of the palmitoyltransferase DHHC6 in mediating CD36 palmitoylation, thus aggravates foam cell formation and atherogenesis [83,84]. We verified this notion using different approaches and obtained the similar result. Truncating the SH3 binding domain in SelK causes a tremendous decrease in CD36 palmitoylation and surface expression in HepG2 cells. Furthermore, a truncated SelK SH3 binding domain reduces the integration of CD36 into COPII, induces the mitigation of CD36 subcellular trafficking and may ameliorate NAFLD in the mouse liver. Consistent with the data reported by Fredericks et al., DHHC6 and SelK form a complex in the ER membrane through the SH3 domain and facilitate palmitoylation of IP3R [24]. This example could provide insights for understanding the signaling functions of palmitoylation in numerous other cell biological or pathological processes.

5. Conclusion

Taken together, our data provide experimental evidence suggesting that selenoprotein K is a novel key factor which facilitates CD36 subcellular trafficking and increases hepatic lipid accumulation. Furthermore, our study may shed light on the selenium status of and selenium supplements for NAFLD patients.

Author contributions

MYY designed the experiments, analyzed the data, prepared figures and wrote the draft of the manuscript. MYY performed the experiments with the help of FW, MLG, MYC, YZ, WZ, DYL and LW. YXC supervised
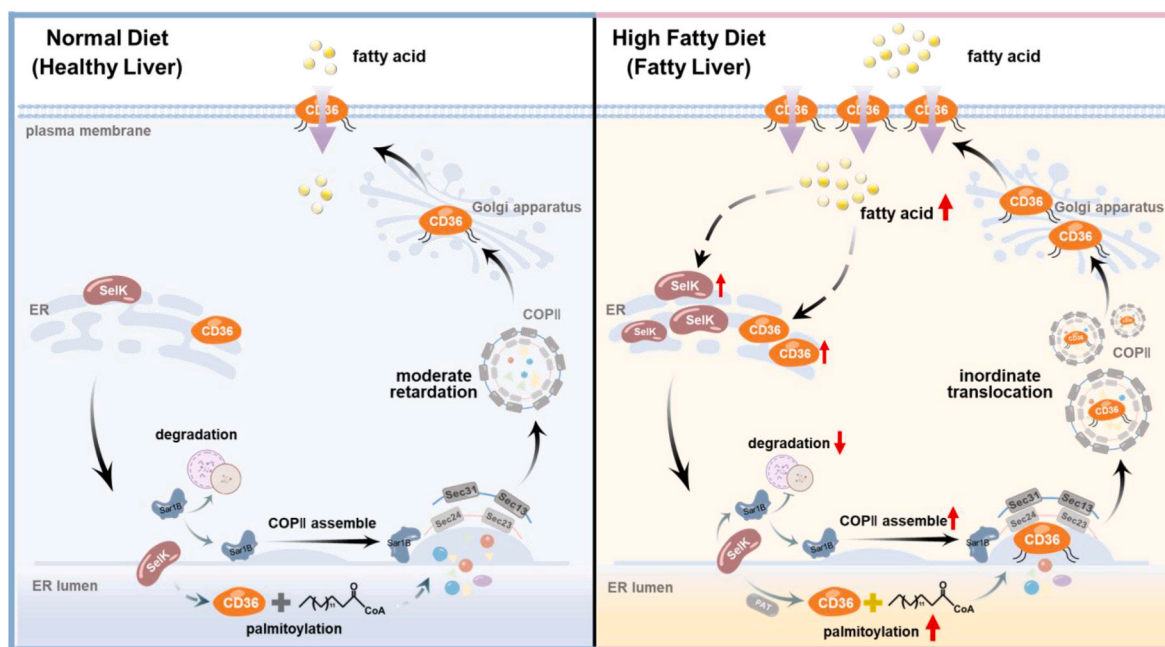

Fig. 10. Schematic diagram of the role of SelK in hepatic steatosis
The increased SelK disturbs the moderate degradation of Sar1B for mediating COPII formation resulting in significant exacerbation of CD36 subcellular trafficking and lipid accumulation in hepatocytes.

this work and edited and revised manuscript. XZR and YXC initiated the project, design the experiments and approved the final version of manuscript.

Data availability

Data will be made available on request.

Appendix A. Supplementary data

Supplementary data to this article can be found online at https://doi.org/10.1016/j.redox.2022.102500.

References

[1] Q. Ye, B. Zou, Y.H. Yeo, J. Li, D.Q. Huang, Y. Wu, H. Yang, C. Liu, L.Y. Kam, X.X. E. Tan, N. Chien, S. Trinh, L. Henry, C.D. Stave, T. Hosaka, R.C. Cheung, M. H. Nguyen, Global prevalence, incidence, and outcomes of non-obese or lean non-alcoholic fatty liver disease: a systematic review and meta-analysis, Lancet Gastroent. Hepatol. 5 (2020) 739–752.

[2] J.V. Lazarus, H.E. Mark, M. Villota-Rivas, A. Palayew, P. Carrieri, M. Colombo, M. Ekstedt, G. Esmat, J. George, G. Marchesini, K. Novak, P. Ocama, V. Ratziu, H. Razavi, M. Romero-Gómez, M. Silva, C.W. Spearman, F. Tacke, E.A. Tsochatzis, Y. Yilmaz, Z.M. Younossi, V.W. Wong, S. Zelber-Sagi, H. Cortez-Pinto, Q.M. Anstee, The global NAFLD policy review and preparedness index: are countries ready to address this silent public health challenge? J. Hepatol. 76 (2022) 771–780.

[3] M. Eslam, L. Valenti, S. Romeo, Genetics and Epigenetics of NAFLD and NASH: Clinical Impact.

[4] M. Eslam, L. Valenti, S. Romeo, Genetics and epigenetics of NAFLD and NASH: clinical impact, J. Hepatol. 68 (2018) 268–279.

[5] J.F.C. Glatz, J. Luiken, Dynamic role of the transmembrane glycoprotein CD36 (SR-B2) in cellular fatty acid uptake and utilization, J. Lipid Res. 59 (2018) 1084–1093.

[6] U. Karunakaran, S. Elumalai, J.S. Moon, K.C. Won, CD36 signal transduction in metabolic diseases: novel insights and therapeutic targeting, Cells 10 (2021).

[7] N.A. Abumrad, A.G. Cabodevilla, D. Samovski, T. Pietka, D. Basu, I.J. Goldberg, Endothelial Cell Receptors in Tissue Lipid Uptake and Metabolism.

[8] N.A. Abumrad, A.G. Cabodevilla, D. Samovski, T. Pietka, D. Basu, I.J. Goldberg, Endothelial cell receptors in tissue lipid uptake and metabolism, Circ. Res. 128 (2021) 433–450.

[9] P. Rada, A. Gonzalez-Rodriguez, C. Garcia-Monzon, A.M. Valverde, Understanding lipotoxicity in NAFLD pathogenesis: is CD36 a key driver? Cell Death Dis. 11 (2020) 802.

[10] L. Zhao, C. Zhang, X. Luo, P. Wang, W. Zhou, S. Zhong, Y. Xie, Y. Jiang, P. Yang, R. Tang, Q. Pan, A.R. Hall, T.V. Luong, J. Fan, Z. Varghese, J.F. Moorhead, M. Pinzani, Y. Chen, X.Z. Ruan, CD36 palmitoylation disrupts free fatty acid metabolism and promotes tissue inflammation in non-alcoholic steatohepatitis, J. Hepatol. 69 (2018) 705–717.

[11] S. Zeng, F. Wu, M. Chen, Y. Li, M. You, Y. Zhang, P. Yang, L. Wei, X.Z. Ruan, L. Zhao, Y. Chen, Inhibition of Fatty Acid Translocase (FAT/CD36) Palmitoylation Enhances Hepatic Fatty Acid β-Oxidation by Increasing its Localization to Mitochondria and Interaction with Long-Chain Acyl-CoA Synthetase 1, Antioxid Redox Signal, 2022.

[12] G.A. Thompson, H. Okuyama, Lipid-linked proteins of plants, Prog. Lipid Res. 39 (2000) 19–39.

[13] A. Patwardhan, N. Cheng, J. Trejo, Post-translational modifications of G protein-coupled receptors control cellular signaling dynamics in space and time, Pharmacol. Rev. 73 (2021) 120–151.

[14] J. Wang, J.W. Hao, X. Wang, H. Guo, H.H. Sun, X.Y. Lai, L.Y. Liu, M. Zhu, H. Y. Wang, Y.F. Li, L.Y. Yu, C. Xie, H.R. Wang, W. Mo, H.M. Zhou, S. Chen, G. Liang, T.J. Zhao, DHHC4 and DHHC5 facilitate fatty acid uptake by palmitoylating and targeting CD36 to the plasma membrane, Cell Rep. 26 (2019) 209–221, e205.

[15] L.V. Papp, J. Lu, A. Holmgren, K.K. Khanna, From selenium to selenoproteins: synthesis, identity, and their role in human health, Antioxidants Redox Signal. 9 (2007) 775–806.

[16] G.V. Kryukov, S. Castellano, S.V. Novoselov, A.V. Lobanov, O. Zehtab, R. Guigo, V. N. Gladyshev, Characterization of mammalian selenoproteomes, Science 300 (2003) 1439–1443.

[17] J. Lu, A. Holmgren, Selenoproteins, J. Biol. Chem. 284 (2009) 723–727.

[18] K. Day, L.A. Seale, R.M. Graham, B.R. Cardoso, Selenotranscriptome network in non-alcoholic fatty liver disease, Front. Nutr. 8 (2021), 744825.

[19] S. Verma, F.W. Hoffmann, M. Kumar, Z. Huang, K. Roe, E. Nguyen-Wu, A. S. Hashimoto, P.R. Hoffmann, Selenoprotein K knockout mice exhibit deficient calcium flux in immune cells and impaired immune responses, J. Immunol. 186 (2011) 2127–2137.

[20] G.J. Fredericks, P.R. Hoffmann, Selenoprotein K and protein palmitoylation, Antioxidants Redox Signal. 23 (2015) 854–862.

[21] C. Lu, F. Qiu, H. Zhou, Y. Peng, W. Hao, J. Xu, J. Yuan, S. Wang, B. Qiang, C. Xu, X. Peng, Identification and characterization of selenoprotein K: an antioxidant in cardiomyocytes, FEBS Lett. 580 (2006) 5189–5197.

[22] R.L. Norton, G.J. Fredericks, Z. Huang, J.D. Fay, F.W. Hoffmann, P.R. Hoffmann, Selenoprotein K regulation of palmitoylation and calpain cleavage of ASAP2 is required for efficient FcγR-mediated phagocytosis, J. Leukoc. Biol. 101 (2017) 439–448.

[23] S.Z. Jia, X.W. Xu, Z.H. Zhang, C. Chen, Y.B. Chen, S.L. Huang, Q. Liu, P. R. Hoffmann, G.L. Song, Selenoprotein K deficiency-induced apoptosis: a role for calpain and the ERS pathway, Redox Biol. 47 (2021), 102154.

[24] G.J. Fredericks, F.W. Hoffmann, A.H. Rose, H.J. Osterheld, F.M. Hess, F. Mercier, P. R. Hoffmann, Stable expression and function of the inositol 1,4,5-triphosphate receptor requires palmitoylation by a DHHC6/selenoprotein K complex, Proc. Natl. Acad. Sci. U. S. A. 111 (2014) 16478–16483.

[25] S. Meiler, Y. Baumer, Z. Huang, F.W. Hoffmann, G.J. Fredericks, A.H. Rose, R. L. Norton, P.R. Hoffmann, W.A. Boisvert, Selenoprotein K is required for palmitoylation of CD36 in macrophages: implications in foam cell formation and atherogenesis, J. Leukoc. Biol. 93 (2013) 771–780.

[26] Y. Li, P. Yang, L. Zhao, Y. Chen, X. Zhang, S. Zeng, L. Wei, Z. Varghese, J. F. Moorhead, Y. Chen, X.Z. Ruan, CD36 plays a negative role in the regulation of lipophagy in hepatocytes through an AMPK-dependent pathway, J. Lipid Res. 60 (2019) 844–855.

[27] M.W. Werno, L.H. Chamberlain, S-Acylation of the insulin-responsive aminopeptidase (IRAP): quantitative analysis and identification of modified cysteines, Sci. Rep. 5 (2015), 12413.

[28] C. Hammond, A. Helenius, Quality Control in the Secretory Pathway: Retention of a Misfolded Viral Membrane Glycoprotein Involves Cycling between the ER, Intermediate Compartment, and Golgi Apparatus.

[29] C. Hammond, A. Helenius, Quality control in the secretory pathway: retention of a misfolded viral membrane glycoprotein involves cycling between the ER, intermediate compartment, and Golgi apparatus, J. Cell Biol. 126 (1994) 41–52.

[30] G.N. Huang, W. Zeng, J.Y. Kim, J.P. Yuan, L. Han, S. Muallem, P.F. Worley, STIM1 carboxyl-terminus activates native SOC, I(crac) and TRPC1 channels, Nat. Cell Biol. 8 (2006) 1003–1010.

[31] C. Barlowe, COPII and selective export from the endoplasmic reticulum, Biochim. Biophys. Acta 1404 (1998) 67–76.

[32] T. Szul, E. Sztul, COPII and COPI traffic at the ER-Golgi interface, Physiology 26 (2011) 348–364.

[33] D. Jensen, R. Schekman, COPII-mediated vesicle formation at a glance, J. Cell Sci. 124 (2011) 1–4.

[34] C. Barlowe, L. Orci, T. Yeung, M. Hosobuchi, S. Hamamoto, N. Salama, M. F. Rexach, M. Ravazzola, M. Amherdt, R. Schekman, COPII: a membrane coat formed by Sec proteins that drive vesicle budding from the endoplasmic reticulum, Cell 77 (1994) 895–907.

[35] A. Budnik, D.J. Stephens, ER exit sites–localization and control of COPII vesicle formation, FEBS Lett. 583 (2009) 3796–3803.

[36] S.I. Bannykh, T. Rowe, W.E. Balch, The organization of endoplasmic reticulum export complexes, J. Cell Biol. 135 (1996) 19–35.

[37] X. Bi, R.A. Corpina, J. Goldberg, Structure of the Sec23/24-Sar1 pre-budding complex of the COPII vesicle coat, Nature 419 (2002) 271–277.

[38] E. Miller, B. Antonny, S. Hamamoto, R. Schekman, Cargo selection into COPII vesicles is driven by the Sec24p subunit, EMBO J. 21 (2002) 6105–6113.

[39] K. Matsuoka, L. Orci, M. Amherdt, S.Y. Bednarek, S. Hamamoto, R. Schekman, T. Yeung, COPII-coated vesicle formation reconstituted with purified coat proteins and chemically defined liposomes, Cell 93 (1998) 263–275.

[40] S. Du, J. Zhou, Y. Jia, K. Huang, SelK is a novel ER stress-regulated protein and protects HepG2 cells from ER stress agent-induced apoptosis, Arch. Biochem. Biophys. 502 (2010) 137–143.

[41] V.A. Shchedrina, R.A. Everley, Y. Zhang, S.P. Gygi, D.L. Hatfield, V.N. Gladyshev, Selenoprotein K binds multiprotein complexes and is involved in the regulation of endoplasmic reticulum homeostasis, J. Biol. Chem. 286 (2011) 42937–42948.

[42] C. Barlowe, R. Schekman, SEC12 encodes a guanine-nucleotide-exchange factor essential for transport vesicle budding from the ER, Nature 365 (1993) 347–349.

[43] E. Futai, S. Hamamoto, L. Orci, R. Schekman, GTP/GDP exchange by Sec12p enables COPII vesicle bud formation on synthetic liposomes, EMBO J. 23 (2004) 4146–4155.

[44] T.C. Stadtman, Selenium biochemistry, Science 183 (1974) 915–922.

[45] K. Buday, M. Conrad, Emerging roles for non-selenium containing ER-resident glutathione peroxidases in cell signaling and disease, Biol. Chem. 402 (2021) 271–287.

[46] J. Zhang, D. Duan, A. Osama, J. Fang, Natural molecules targeting thioredoxin system and their therapeutic potential, Antioxidants Redox Signal. 34 (2021) 1083–1107.

[47] Y. Zhang, Y.J. Roh, S.-J. Han, I. Park, H.M. Lee, Y.S. Ok, B.C. Lee, S.-R. Lee, Role of selenoproteins in redox regulation of signaling and the antioxidant system: a review, Antioxidants 9 (2020).

[48] M.P. Rayman, Selenium and human health, Lancet (London, England) 379 (2012) 1256–1268.

[49] J.C. Avery, P.R. Hoffmann, Selenium, selenoproteins, and immunity, Nutrients 10 (2018).

[50] S.A. Polyzos, J. Kountouras, A. Goulas, L. Duntas, Selenium and selenoprotein P in nonalcoholic fatty liver disease, Hormones (Basel) 19 (2020) 61–72.

[51] R.C.R. Meex, M.J. Watt, Hepatokines: linking nonalcoholic fatty liver disease and insulin resistance, Nature reviews, Endocrinology 13 (2017) 509–520.

[52] H.K. Berthold, B. Michalke, W. Krone, E. Guallar, I. Gouni-Berthold, Influence of serum selenium concentrations on hypertension: the Lipid Analytic Cologne cross-sectional study, J. Hypertens. 30 (2012) 1328–1335.

[53] K. Christensen, M. Werner, K. Malecki, Serum selenium and lipid levels: associations observed in the national health and nutrition examination survey (NHANES) 2011–2012, Environ. Res. 140 (2015) 76–84.

[54] H. Steinbrenner, L.H. Duntas, M.P. Rayman, The role of selenium in type-2 diabetes mellitus and its metabolic comorbidities, Redox Biol. 50 (2022), 102236.

[55] M.P. Rayman, Selenium and human health, Lancet 379 (2012) 1256–1268.

[56] X. Wang, W. Zhang, H. Chen, N. Liao, Z. Wang, X. Zhang, C. Hai, High selenium impairs hepatic insulin sensitivity through opposite regulation of ROS, Toxicol. Lett. 224 (2014) 16–23.

[57] R. Knight, V.L. Marlatt, J.A. Baker, B.P. Lo, A.M.H. deBruyn, J.R. Elphick, C. J. Martyniuk, Dietary selenium disrupts hepatic triglyceride stores and transcriptional networks associated with growth and Notch signaling in juvenile rainbow trout, Aquat. Toxicol. 180 (2016) 103–114.

[58] C. Fürnsinn, R. Englisch, K. Ebner, P. Nowotny, C. Vogl, W. Waldhäusl, Insulin-like vs. non-insulin-like stimulation of glucose metabolism by vanadium, tungsten, and selenium compounds in rat muscle, Life Sci. 59 (1996) 1989–2000.

[59] Z. Zhao, M. Barcus, J. Kim, K.L. Lum, C. Mills, X.G. Lei, High dietary selenium intake alters lipid metabolism and protein synthesis in liver and muscle of pigs, J. Nutr. 146 (2016) 1625–1633.

[60] Z. Yang, C. Yan, G. Liu, Y. Niu, W. Zhang, S. Lu, X. Li, H. Zhang, G. Ning, J. Fan, L. Qin, Q. Su, Plasma selenium levels and nonalcoholic fatty liver disease in Chinese adults: a cross-sectional analysis, Sci. Rep. 6 (2016), 37288.

[61] X. Wang, Y.A. Seo, S.K. Park, Serum selenium and non-alcoholic fatty liver disease (NAFLD) in U.S. adults: National Health and Nutrition Examination Survey (NHANES) 2011-2016, Environ. Res. 197 (2021), 111190.

[62] T. Urbano, T. Filippini, D. Lasagni, T. De Luca, P. Grill, S. Sucato, E. Polledri, G. Djeukeu Noumbi, M. Malavolti, A. Santachiara, T.A. Pertinhez, R. Baricchi, S. Fustinoni, B. Michalke, M. Vinceti, Association of Urinary and dietary selenium and of serum selenium species with serum alanine aminotransferase in a healthy Italian population, Antioxidants 10 (2021).

[63] M.P. Suppli, K.T.G. Rigbolt, S.S. Veidal, S. Heebøll, P.L. Eriksen, M. Demant, J. I. Bagger, J.C. Nielsen, D. Oró, S.W. Thrane, A. Lund, C. Strandberg, M.J. Kønig, T. Vilsbøll, N. Vrang, K.L. Thomsen, H. Grønbæk, J. Jelsing, H.H. Hansen, F. K. Knop, Hepatic transcriptome signatures in patients with varying degrees of nonalcoholic fatty liver disease compared with healthy normal-weight individuals, Am. J. Physiol. Gastrointest. Liver Physiol. 316 (2019) G462–g472.

[64] L. Fagerberg, B.M. Hallström, P. Oksvold, C. Kampf, D. Djureinovic, J. Odeberg, M. Habuka, S. Tahmasebpoor, A. Danielsson, K. Edlund, A. Asplund, E. Sjöstedt, E. Lundberg, C.A. Szigyarto, M. Skogs, J.O. Takanen, H. Berling, H. Tegel, J. Mulder, P. Nilsson, J.M. Schwenk, C. Lindskog, F. Danielsson, A. Mardinoglu, A. Sivertsson, K. von Feilitzen, M. Forsberg, M. Zwahlen, I. Olsson, S. Navani, M. Huss, J. Nielsen, F. Ponten, M. Uhlén, Analysis of the human tissue-specific expression by genome-wide integration of transcriptomics and antibody-based proteomics, Mol. Cell. Proteomics : MCP 13 (2014) 397–406.

[65] S. Wang, X. Zhao, Q. Liu, Y. Wang, S. Li, S. Xu, Selenoprotein K protects skeletal muscle from damage and is required for satellite cells-mediated myogenic differentiation, Redox Biol. 50 (2022), 102255.

[66] C. Jehan, D. Cartier, C. Bucharles, Y. Anouar, I. Lihrmann, Emerging roles of ER-resident selenoproteins in brain physiology and physiopathology, Redox Biol. 55 (2022), 102412.

[67] M.P. Marciel, P.R. Hoffmann, Molecular mechanisms by which selenoprotein K regulates immunity and cancer, Biol. Trace Elem. Res. 192 (2019) 60–68.

[68] L. Cao, L. Zhang, H. Zeng, R.T. Wu, T.L. Wu, W.H. Cheng, Analyses of selenotranscriptomes and selenium concentrations in response to dietary selenium deficiency and age reveal common and distinct patterns by tissue and sex in telomere-dysfunctional mice, J. Nutr. 147 (2017) 1858–1866.

[69] L.K. Steinbusch, R.W. Schwenk, D.M. Ouwens, M. Diamant, J.F. Glatz, J.J. Luiken, Subcellular trafficking of the substrate transporters GLUT4 and CD36 in cardiomyocytes, Cell. Mol. Life Sci. 68 (2011) 2525–2538.

[70] J.F.C. Glatz, M. Nabben, J.J.F.P. Luiken, CD36 (SR-B2) as master regulator of cellular fatty acid homeostasis, Curr. Opin. Lipidol. 33 (2022) 103–111.

[71] J. Bethune, F.T. Wieland, Assembly of COPI and COPII vesicular coat proteins on membranes, Annu. Rev. Biophys. 47 (2018) 63–83.

[72] Y.N. Wang, H.H. Lee, J.L. Hsu, D. Yu, M.C. Hung, The impact of PD-L1 N-linked glycosylation on cancer therapy and clinical diagnosis, J. Biomed. Sci. 27 (2020) 77.

[73] C. Aicart-Ramos, R.A. Valero, I. Rodriguez-Crespo, Protein palmitoylation and subcellular trafficking, Biochim. Biophys. Acta 1808 (2011) 2981–2994.

[74] M.E. Linder, B.C. Jennings, Mechanism and function of DHHC S-acyltransferases, Biochem. Soc. Trans. 41 (2013) 29–34.

[75] H. Jiang, X. Zhang, X. Chen, P. Aramsangtienchai, Z. Tong, H. Lin, Protein lipidation: occurrence, mechanisms, biological functions, and enabling technologies, Chem. Rev. 118 (2018) 919–988.

[76] C.D. Gottlieb, M.E. Linder, Structure and function of DHHC protein S-acyltransferases, Biochem. Soc. Trans. 45 (2017) 923–928.

[77] C. Busquets-Hernández, G. Triola, Palmitoylation as a key regulator of Ras localization and function, Front. Mol. Biosci. 8 (2021), 659861.

[78] Z. Zhang, X. Li, F. Yang, C. Chen, P. Liu, Y. Ren, P. Sun, Z. Wang, Y. You, Y.X. Zeng, X. Li, DHHC9-mediated GLUT1 S-palmitoylation promotes glioblastoma glycolysis and tumorigenesis, Nat. Commun. 12 (2021) 5872.

[79] L.H. Chamberlain, K. Lemonidis, M. Sanchez-Perez, M.W. Werno, O.A. Gorleku, J. Greaves, Palmitoylation and the trafficking of peripheral membrane proteins, Biochem. Soc. Trans. 41 (2013) 62–66.

[80] D.A. Mitchell, A. Vasudevan, M.E. Linder, R.J. Deschenes, Thematic review series: lipid Posttranslational Modifications. Protein palmitoylation by a family of DHHC protein S-acyltransferases, JLR (J. Lipid Res.) 47 (2006) 1118–1127.

[81] D.T. Lin, E. Conibear, Enzymatic protein depalmitoylation by acyl protein thioesterases, Biochem. Soc. Trans. 43 (2015) 193–198.

[82] C. Salaun, J. Greaves, L.H. Chamberlain, The intracellular dynamic of protein palmitoylation, J. Cell Biol. 191 (2010) 1229–1238.

[83] S. Meiler, Y. Baumer, Z. Huang, F.W. Hoffmann, G.J. Fredericks, A.H. Rose, R. L. Norton, P.R. Hoffmann, W.A. Boisvert, Selenoprotein K is required for palmitoylation of CD36 in macrophages: implications in foam cell formation and atherogenesis, J. Leukoc. Biol. 93 (2013) 771–780.

[84] Y. Zhang, D. Dong, X. Xu, H. He, Y. Zhu, T. Lei, H. Ou, Oxidized high-density lipoprotein promotes CD36 palmitoylation and increases lipid uptake in macrophages, J. Biol. Chem. 298 (2022), 102000.

Abbreviations:

selenoprotein K: (SelK)
selenium: (Se)
nonalcoholic fatty liver disease: (NAFLD)
high-fat diet: (HFD)
cluster of differentiation 36: (CD36)
coat protein complex ‖ vesicle: (COPII vesicle)
Secretion Associated Ras Related GTPase 1B: (Sar1B)
endoplasmic reticulum: (ER)
Golgi apparatus: (Golgi)
ER associated degradation: (ERAD)
fatty acid: (FA)
palmitic acid: (PA)
normal chow diet: (NCD)
Src homology 3 domain: (SH3)
brefeldin A: (BFA)